

Magnetic and glassy transitions in the square-lattice XY model with random phase shifts

Vincenzo Alba¹, Andrea Pelissetto² and Ettore Vicari³

¹ Scuola Normale Superiore and INFN, I-56126 Pisa, Italy

² Dipartimento di Fisica dell'Università di Roma "La Sapienza" and INFN, I-00185 Roma, Italy

³ Dipartimento di Fisica dell'Università di Pisa and INFN, I-56127 Pisa, Italy

E-mail: Vincenzo.Alba@sns.it, Andrea.Pelissetto@roma1.infn.it, Ettore.Vicari@df.unipi.it

Abstract.

We investigate the magnetic and glassy transitions of the square-lattice XY model in the presence of random phase shifts. We consider two different random-shift distributions: the Gaussian distribution and a slightly different distribution (cosine distribution) which allows the exact determination of the Nishimori line where magnetic and overlap correlation functions are equal. We perform Monte Carlo simulations for several values of the temperature and of the variance of the disorder distribution, in the paramagnetic phase close to the magnetic and glassy transition lines. We find that, along the transition line separating the paramagnetic and the quasi-long-range order phases, magnetic correlation functions show a universal Kosterlitz-Thouless behavior as in the pure XY model, while overlap correlations show a disorder-dependent critical behavior. This behavior is observed up to a multicritical point which, in the cosine model, lies on the Nishimori line. Finally, for large values of the disorder variance, we observe a universal zero-temperature glassy critical transition, which is in the same universality class as that occurring in the gauge-glass model.

1. Introduction

The two-dimensional XY model with random phase shifts (RPXY) describes the thermodynamic behavior of several disordered systems, such as Josephson junction arrays with geometrical disorder [1, 2], magnetic systems with random Dzyaloshinskii-Moriya interactions [3], crystal systems on disordered substrates [4], and vortex glasses in high- T_c cuprate superconductors [5]. See [6, 7] for recent reviews. The RPXY model is defined by the partition function

$$\begin{aligned} Z(\{A\}) &= \exp(-\mathcal{H}/T), \\ \mathcal{H} &= - \sum_{\langle xy \rangle} \text{Re} \bar{\psi}_x U_{xy} \psi_y = - \sum_{\langle xy \rangle} \cos(\theta_x - \theta_y - A_{xy}), \end{aligned} \quad (1)$$

where $\psi_x \equiv e^{i\theta_x}$, $U_{xy} \equiv e^{iA_{xy}}$, and the sum runs over the bonds $\langle xy \rangle$ of a square lattice. The phases A_{xy} are uncorrelated quenched random variables with zero average. In most studies they are distributed with Gaussian probability

$$P_G(A_{xy}) \propto \exp\left(-\frac{A_{xy}^2}{2\sigma}\right). \quad (2)$$

We denote the RPXY model with distribution (2) by GRPXY. We also consider the RPXY model with distribution (cosine model)

$$P_C(A_{xy}) \propto \exp\left(\frac{\cos A_{xy}}{\sigma}\right), \quad (3)$$

which we denote by CRPXY. Such a model is particularly interesting because the distribution (3) allows some exact calculations along the so-called Nishimori (N) line $T \equiv 1/\beta = \sigma$ [8, 9]. In both GRPXY and CRPXY models the pure XY model is recovered in the limit $\sigma \rightarrow 0$, while the so-called gauge glass model [10] with uniformly distributed phase shifts is obtained in the limit $\sigma \rightarrow \infty$.

The nature of the different phases arising when varying the temperature T and the disorder parameter σ and the critical behavior at the phase transitions have been investigated in many theoretical and experimental works [3, 1, 2, 4, 5, 6, 7, 8, 9, 10, 11, 12, 13, 14, 15, 16, 17, 18, 19, 20, 21, 22, 23, 24, 25, 26, 27, 28, 29, 30, 31, 32, 33, 34, 35, 36, 37, 39, 38, 40, 41, 42, 43, 44, 45, 46, 47, 48, 49, 50, 51, 52, 53, 54, 55]. In spite of that, a conclusive picture of the phase diagram and of the critical behaviors has not been achieved yet.

The expected T - σ phase diagram for the GRPXY and CRPXY models, which is sketched in Fig. 1, presents two finite-temperature phases: a paramagnetic phase and a low-temperature phase characterized by quasi-long-range order (QLRO) for sufficiently small values of σ ; see, e.g., [55] and references therein. The paramagnetic phase is separated from the QLRO phase by a transition line, which starts from the pure XY point (denoted by P in Fig. 1) at $(\sigma = 0, T = T_{XY} \approx 0.893)$ and ends at a zero-temperature disorder-induced transition denoted by D at $(\sigma_D, T = 0)$. The QLRO phase extends up to a maximum value σ_M of the disorder parameter, which is related to the point $M \equiv (\sigma_M, T_M)$, where the tangent to the transition line is parallel to the

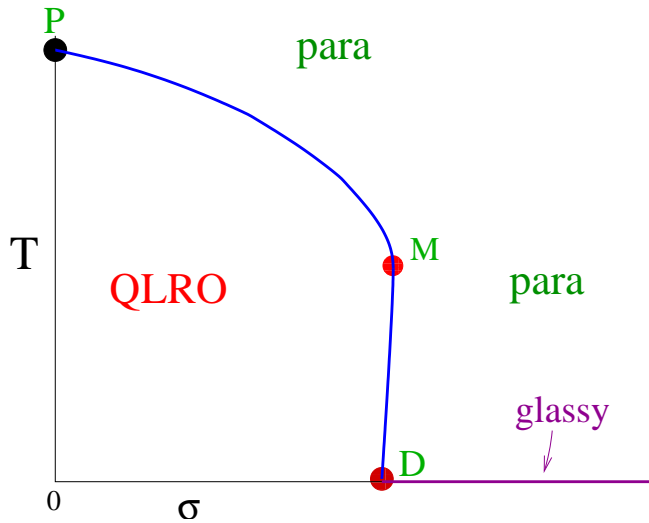


Figure 1. Phase diagram of RPXY models as a function of T and of the disorder-distribution variance σ .

T axis. No long-range glassy order can exist at finite temperature for any value of σ , including the gauge-glass limit $\sigma \rightarrow \infty$ [21, 22]. Several numerical studies of the gauge-glass XY model [5, 19, 36, 43, 45, 46, 49, 50, 51] support a zero-temperature glassy transition. A more complete discussion of the known features of the phase diagram will be reported below.

In this paper we investigate several controversial issues concerning the critical behavior at the magnetic and glassy transitions in RPXY models. In particular, we will check whether the critical behavior along the paramagnetic-QLRO transition line is universal and belongs to the universality class of the pure XY model, whether there is a multicritical point along the paramagnetic-QLRO transition line, and, finally, whether the $T = 0$ glassy transition extends from $\sigma = \infty$ to $\sigma = \sigma_D$, see Fig. 1, and belongs to the same universality class as that in the XY gauge-glass model. For this purpose, we perform Monte Carlo (MC) simulations of the GRPXY and CRPXY models for several values of the temperature and of the variance σ , approaching the magnetic and glassy transition lines from the paramagnetic phase. As we shall see, our results for the CRPXY model provide a robust evidence for a universal Kosterlitz-Thouless (KT) behavior of the magnetic correlations along the paramagnetic-QLRO transition line from the pure XY point P to the point M where the transition line runs parallel to the T axis and magnetic and overlap correlations are equal. Along the line the magnetic correlation length ξ behaves as $\ln \xi \sim u_t^{-1/2}$, where u_t is the thermal scaling field, and the magnetic susceptibility as $\chi \sim \xi^{7/4}$ (corresponding to $\eta = 1/4$). On the other hand, the behavior of the overlap correlations appears to be σ dependent along this transition line. Moreover, the numerical results for the CRPXY model indicate that the point M is multicritical. We conjecture that these conclusions hold for any RPXY model. In all cases we expect that the paramagnetic-QLRO transition line is divided into two parts by a multicritical point M , where magnetic and overlap correlations have the same critical

behavior, though they are not equal. At variance with what happens in the CRPXY model, the point M is not expected to coincide with the point in which the tangent to the transition line is parallel to the T axis: this coincidence should be a unique feature of the CRPXY model. Then, from P to M we expect any RPXY model to behave as the CRPXY, that is a KT behavior for magnetic correlations and a σ dependent behavior for disorder-related quantities. The universality of the behavior has been confirmed by our numerical results for the GRPXY model.

Finally, we have investigated the critical behavior for large values of σ . Our numerical results provide strong evidence for a universal zero-temperature glassy transition for $\sigma > \sigma_D$. For $T \rightarrow 0$ overlap correlation functions are critical, and, in particular, the corresponding correlation length ξ_o diverges as $\xi_o \sim T^{-\nu}$ when $T \rightarrow 0$ with $\nu = 2.5(1)$.

This paper is organized as follows. In Sec. 2 we review the known results for the phase diagram and for the critical behavior of the RPXY models. Sec. 3 provides the definitions of the quantities considered in our numerical work. In Sec. 4 we study the critical behavior along the thermal paramagnetic-QLRO transition line which starts at the pure XY point P and ends at multicritical point M . In Sec. 5 we discuss critical behavior along the N line of the CRPXY model and show that the point M where the N line intersects the critical line is multicritical. In Sec. 6 we investigate the glassy critical behavior at $T = 0$ for $\sigma > \sigma_D$. Finally, in Sec. 7 we draw our conclusions. There are also several appendices. Appendix A reports some details of the MC simulations. Appendix B is devoted to a careful analysis of the KT renormalization-group (RG) equations and of the corresponding RG flow. We derive the most general form of the β function for the sine-Gordon model and discuss the structure of the scaling corrections in the XY model. These results are used in the discussion of the behavior at the paramagnetic-QLRO transition. In Appendix C we discuss some features of the critical behavior at a multicritical point. In Appendix D we briefly discuss the RG equations in the presence of randomness. Finally, in Appendix E we report some analytical results for the magnetic correlations in the gauge-glass model.

2. The phase diagram

In Fig. 1 we show the expected T - σ phase diagram of the RPXY models. In the absence of disorder ($\sigma = 0$) the model shows a high- T paramagnetic phase and a low- T phase characterized by QLRO controlled by a line of Gaussian fixed points, where the spin-spin correlation function $\langle \bar{\psi}_x \psi_y \rangle$ decays as $1/r^{\eta(T)}$ for $r \equiv |x - y| \rightarrow \infty$, with η depending on T . The two phases are separated by a Kosterlitz-Thouless (KT) transition [56] at [57] $\beta_{XY} \equiv 1/T_{XY} = 1.1199(1)$. For $\tau \equiv T/T_{XY} - 1 \rightarrow 0^+$, the correlation length and the magnetic susceptibility diverge exponentially as $\ln \xi \sim \tau^{-1/2}$ and $\chi \sim \xi^{7/4}$, respectively. An interesting question is whether these features change in the presence of random phase shifts.

The low-temperature phase of RPXY models shows QLRO for sufficiently small

values of σ . The universal features of the long-distance behavior are explained by the random spin-wave theory [3], obtained by replacing

$$\cos(\theta_x - \theta_y - A_{xy}) \longrightarrow 1 - \frac{1}{2}(\theta_x - \theta_y + A_{xy})^2 \quad (4)$$

in Hamiltonian (1). This scenario has been accurately verified by Monte Carlo (MC) simulations in both GRPXY and CRPXY models [55]. The QLRO phase disappears for large values of σ , see, e.g., [6] and references therein; more precisely, as we shall see, for $\sigma \gtrsim 0.31$ in the case of the CRPXY model.

For $\sigma \rightarrow \infty$ phases are uniformly distributed and one obtains the gauge-glass model. Even if this model has been much investigated [5, 10, 14, 15, 16, 17, 18, 19, 21, 22, 25, 26, 29, 32, 33, 34, 36, 38, 40, 41, 43, 44, 45, 46, 47, 48, 49, 50, 51, 52, 54], its phase diagram and critical behavior are still controversial. No long-range glassy order can exist at finite temperature [21, 22]. However, this does not exclude more exotic low-temperature glassy phases [40, 47], for example a phase characterized by glassy QLRO. Many numerical works at finite and zero temperature support a zero-temperature transition [5, 19, 36, 43, 45, 46, 49, 50, 51]. According to this scenario, the correlation length determined from the overlap correlation function diverges as $\xi_o \sim T^{-\nu}$ when approaching the critical point $T = 0$. The critical exponent ν has been estimated by finite-temperature Monte Carlo (MC) simulations, obtaining [45] $1/\nu = 0.39(3)$ and [49] $1/\nu = 0.36(3)$. The exponent ν is related to the $T = 0$ stiffness exponent θ by $\theta = -1/\nu$. The $T = 0$ numerical calculations of [43] and [51] provided the estimates $\theta = -0.36(1)$ and $\theta \approx -0.45$ respectively, which are consistent with the finite-temperature estimates of ν . The $T = 0$ transition scenario has been questioned in [40, 41, 44, 47, 48, 52, 53, 54], which provide some numerical and experimental (for Josephson-junction arrays with positional disorder [53]) evidence for the existence of a finite-temperature transition at $T \approx 0.2$, with a low-temperature glassy phase characterized by frozen vortices and glassy QLRO.

Other features of the phase diagram are better discussed within the CRPXY model, characterized by the random phase-shift distribution (3), because of the existence of exact results along the so-called Nishimori (N) line [8, 9]

$$T \equiv 1/\beta = \sigma. \quad (5)$$

Along the N line the energy density E is known exactly:

$$E \equiv \frac{1}{V}[\langle \mathcal{H} \rangle] = -2 \frac{I_1(\beta)}{I_0(\beta)}, \quad (6)$$

where $I_0(\beta)$ and $I_1(\beta)$ are modified Bessel functions. Moreover, the spin-spin and overlap correlation functions are equal:

$$[\langle \bar{\psi}_x \psi_y \rangle] = [|\langle \bar{\psi}_x \psi_y \rangle|^2]. \quad (7)$$

As already noted in [9], the N line should play an important role in the phase diagram, because it is expected to mark the crossover between the magnetic-dominated region and the disorder-dominated one.

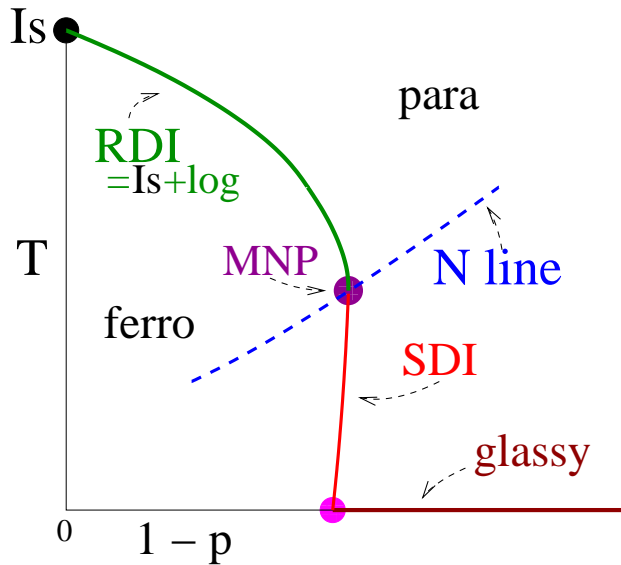


Figure 2. Phase diagram of the $\pm J$ (Edwards-Anderson) Ising model on the square lattice. The phase diagram is symmetric under $p \rightarrow 1 - p$.

In the GRPXY and CRPXY models, the paramagnetic phase is separated from the magnetic QLRO phase by a transition line, which starts from the pure XY point (denoted by P in Fig. 1) at $(\sigma = 0, T = T_{XY} \approx 0.893)$ and ends at a $T = 0$ transition point induced by disorder (denoted by D) at $(\sigma_D, T = 0)$, where $\sigma_D > 0$.[‡] An important result has been proven for the CRPXY model [8]: the critical value σ_M of σ along the N line is an upper bound for the values of σ where magnetic QLRO can exist. Therefore, at the critical point $M \equiv (\sigma_M, T_M)$ the tangent to the critical line should be parallel to the T axis; moreover, the critical value σ_D at $T = 0$ must satisfy $\sigma_D \leq \sigma_M$.

It is worth noting how similar the phase diagrams of the CRPXY model and of the square-lattice $\pm J$ Ising model in the T - p plane are, see Figs. 1 and 2, respectively. The square lattice $\pm J$ (Edwards-Anderson) Ising model is defined by the Hamiltonian

$$\mathcal{H}_{\pm J} = - \sum_{\langle xy \rangle} J_{xy} \sigma_x \sigma_y, \quad (8)$$

where $\sigma_x = \pm 1$, the sum is over pairs of nearest-neighbor sites of a square lattice, and J_{xy} are uncorrelated quenched random variables, taking values $\pm J$ with probability distribution $P(J_{xy}) = p\delta(J_{xy} - J) + (1-p)\delta(J_{xy} + J)$. This model presents an analogous N line [58] in the T - p phase diagram, defined by $\tanh(1/T) - 2p + 1 = 0$. The transition point along the N line is a multicritical point (MNP) [59, 60]. Moreover, the critical behavior for $T > T_{MNP}$ and $T < T_{MNP}$ is different. From the pure Ising point at $p = 1$

[‡] We mention that the first renormalization-group (RG) analyses based on a Coulomb-gas description [3] predicted $\sigma_D = 0$, but it was later clarified that this was an artefact of the approximations. Indeed, experimental [11] and numerical works [11, 12, 13, 30] as well as refinings of the RG arguments [8, 23, 27, 28, 31, 35], have shown the absence of a reentrant transition for sufficiently small values of σ .

to the MNP the critical behavior is analogous to that observed in 2D randomly dilute Ising (RDI) models [61]. From the MNP to the $T = 0$ axis the critical behavior belongs to a new strong-disorder Ising (SDI) universality class [62]. Finally, the $T = 0$ end-point of the low-temperature paramagnetic-ferromagnetic transition line is the starting point of a $T = 0$ transition line, characterized by a glassy universal critical behavior [63].

In [8] it was also argued that, in the RPXY models (in particular, in the CRPXY one) the low-temperature paramagnetic-QLRO transition line from the critical point M to the point D runs parallel to the T axis, so that $\sigma_D = \sigma_M$. The same arguments fail in the 2D $\pm J$ Ising model [62, 59, 60, 64, 65], although they provide a good approximation. Thus, they are likely not exact also in the case of the RPXY models, although they may still provide a good approximation, suggesting that $0 < \sigma_M - \sigma_D \ll \sigma_M$.

In the phase diagram reported in Fig. 1, which refers to the CRPXY, we may distinguish two transition lines meeting at point M : the thermal paramagnetic-QLRO transition line from P to M , which can be approached by decreasing the temperature at fixed σ , and the transition line from M to D , which can be instead observed by changing disorder at fixed T for sufficiently low temperatures. As we shall see, our numerical results for the CRPXY model provide some evidence that the point M is multicritical. We conjecture that the same conclusion holds for generic RPXY models, though in the generic case we do not expect the multicritical point M to coincide with the point where the tangent to the critical line is parallel to the T axis.

The phase transition from the paramagnetic to the QLRO phase is generally expected to be of KT type ($\ln \xi$ is expected to have a power-law divergence), but its specific features, for instance the precise form of the power-law behavior and the value of the exponent η , have not been conclusively determined yet. Some numerical results supporting the KT-like behavior were presented in [30]. The disorder-driven $T = 0$ transition at σ_D has been argued [23, 24, 30, 35, 42] to show a KT-like behavior with $\ln \xi \sim (\sigma - \sigma_D)^{-1}$ and $\chi \sim \xi^{2-\eta}$ with $\eta = 1/16$. However, other RG studies [31, 28] obtained a different behavior: $\ln \xi \sim (\sigma - \sigma_D)^{-1/2}$. The value of η associated with the magnetic two-point function has been believed to vary along the critical line [3, 23, 28, 31], from $\eta = 1/4$ of the pure XY model at $\sigma = 0$ to $\eta = 1/16$ at the $T = 0$ transition. As we shall see, our numerical results along the thermal paramagnetic-QLRO transition line, from P to and including M , strongly support $\eta = 1/4$, independently of σ .

In the following sections we investigate some of the open issues of the RPXY models, by performing MC simulations of the GRPXY and CRPXY models close to their magnetic and glassy transition lines. In particular, we investigate the critical behavior at the thermal paramagnetic-QLRO transition line (from point P to the multicritical point), along the N line in the CRPXY model, and at the $T = 0$ glassy transition line for large disorder.

3. Notations

We consider RPXY models defined on square lattices of size L^2 with periodic boundary conditions. We define the magnetic spin-spin correlation function

$$G(x-y) \equiv [\langle \bar{\psi}_x \psi_y \rangle] \quad (9)$$

and the overlap correlation function

$$G_o(x-y) \equiv [|\langle \bar{\psi}_x \psi_y \rangle|^2]. \quad (10)$$

The angular and square brackets indicate the thermal average and the quenched average over disorder, respectively. The latter can also be written in terms of the overlap variables. Given two copies of the system with spins $\psi_x^{(1)}$ and $\psi_x^{(2)}$, we define

$$q_x = \bar{\psi}_x^{(1)} \psi_x^{(2)}, \quad G_o(x-y) = [\langle \bar{q}_x q_y \rangle], \quad (11)$$

where the thermal average is performed over the two systems with the same disorder configuration. We define the magnetic susceptibility $\chi \equiv \sum_x G(x)$, the overlap susceptibility $\chi_o \equiv \sum_x G_o(x)$, and the second-moment correlation lengths

$$\xi^2 \equiv \frac{\tilde{G}(0) - \tilde{G}(q_{\min})}{\hat{q}_{\min}^2 \tilde{G}(q_{\min})}, \quad \xi_o^2 \equiv \frac{\tilde{G}_o(0) - \tilde{G}_o(q_{\min})}{\hat{q}_{\min}^2 \tilde{G}_o(q_{\min})}, \quad (12)$$

where $q_{\min} \equiv (2\pi/L, 0)$, $\hat{q} \equiv 2 \sin q/2$.

We also define the quartic couplings

$$g_4 \equiv -\frac{3\chi_4}{2\chi^2\xi^2}, \quad \chi_4 \equiv \frac{1}{V}[\langle |\mu|^4 \rangle - 2\langle |\mu|^2 \rangle^2], \quad (13)$$

$$g_{22} \equiv -\frac{\chi_{22}}{\chi^2\xi^2}, \quad \chi_{22} \equiv \frac{1}{V}([\langle |\mu|^2 \rangle^2] - [\langle |\mu|^2 \rangle]^2), \quad (14)$$

$$g_c \equiv g_4 + 3g_{22}, \quad (15)$$

where $\mu \equiv \sum_x \psi_x$ and $V = L^2$. Note that for the pure XY model $g_{22} = 0$ and $g_c = g_4$. Finally, we define an overlap quartic coupling g_o as

$$g_o \equiv -\frac{3\bar{\chi}_{4o}}{2\chi_o^2\xi_o^2}, \quad \bar{\chi}_{4o} \equiv \frac{1}{V}[\langle |\mu_o|^4 \rangle] - 2[\langle |\mu_o|^2 \rangle]^2, \quad (16)$$

where $\mu_o \equiv \sum_x q_x$.

4. Critical behavior along the thermal para-QLRO transition line

In this section we study the critical behavior of the RPXY models along the thermal paramagnetic-QLRO transition line, see Fig. 1, which starts at the point P on the $\sigma = 0$ axis and ends at the multicritical point, which belongs to the N line in the CRPXY model. For this purpose, we perform MC simulations of the GRPXY and of the CRPXY model for several values of T and σ in the paramagnetic phase, where the magnetic correlation length ξ is large but finite. Fig. 3 shows the points where the simulations are performed. The MC algorithm is described in Appendix A. We average over a large number of samples, $N_s \approx 10^4$ in most cases. We consider large lattice sizes,

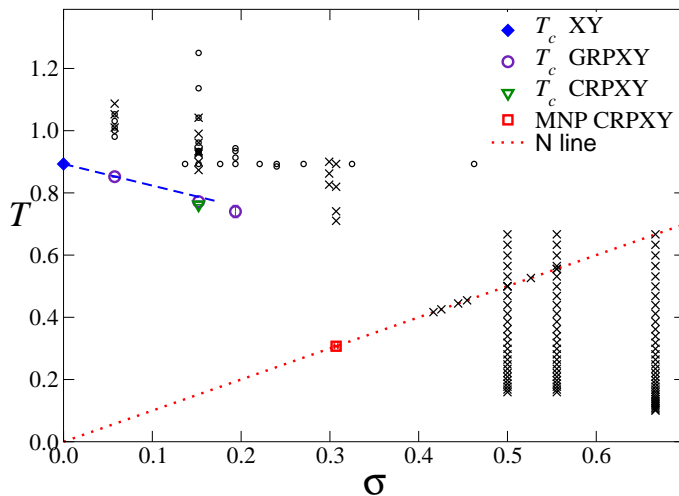


Figure 3. Values of $T \equiv 1/\beta$ and σ where MC data were collected. The circles and crosses refer to the GRPXY and CRPXY models, respectively. The dotted line $T = \sigma$ is the N line for the CRPXY model. We also show some estimates of T_c for the GRPXY and CRPXY models, and the critical point (MNP) of the CRPXY model along the N line. The dashed line is the prediction (27) for the behavior of T_c at small values of σ .

satisfying $L/\xi \gtrsim 10$, in order to make finite-size effects negligible and obtain infinite-volume results. The residual finite-size effects are in all cases smaller than, or at most comparable with, the statistical errors.

In the following we first discuss the critical behavior of the magnetic spin-spin correlation function (9). We show that disorder is apparently irrelevant: for any σ the correlation length diverges following the KT law valid for $\sigma = 0$ and the magnetic susceptibility diverges with critical exponent η equal to $1/4$. Then, we discuss the behavior of observables related to the overlap correlation function (10), finding that the critical behavior of these quantities is apparently σ dependent.

4.1. Critical behavior approaching the pure XY transition point

We wish now to understand the critical behavior along any line that lies in the paramagnetic phase and ends at the pure XY critical point at $\sigma = 0$ and $T = T_{XY}$. For $\sigma = 0$, as T approaches the critical temperature T_{XY} from above (paramagnetic phase), the magnetic correlation length ξ diverges as

$$\ln(\xi/X) = C\tau^{-1/2} + O(\tau^{1/2}), \quad \tau \equiv (T - T_{XY})/T_{XY}, \quad (17)$$

where X and C are nonuniversal constants. In the case of the square-lattice XY model with nearest-neighbor interactions [57] $\beta_{XY} \equiv 1/T_{XY} = 1.1199(1)$, $X = 0.233(3)$ and

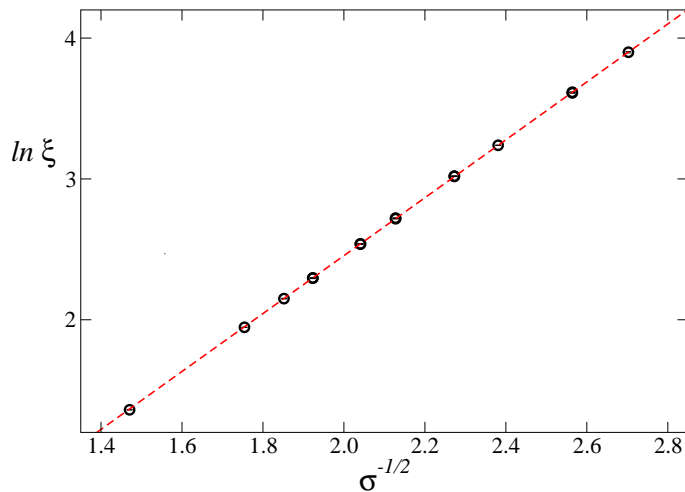


Figure 4. MC estimates of ξ for $\beta = \beta_{XY} = 1.1199$ and several values of σ versus $\sigma^{-1/2}$. The dashed line corresponds to a linear fit to $\ln \xi = C_\sigma \sigma^{-1/2} + b$.

$C = 1.776(4)$.[§] The magnetic susceptibility χ diverges as, see Appendix B,

$$\chi = A_\chi \xi^{7/4} \left[1 + \frac{b_\chi}{\ln(\xi/X)} + O(1/\ln^2 \xi) \right]. \quad (18)$$

Note that while A_χ is a nonuniversal amplitude, the coefficient b_χ of the leading logarithmic corrections is universal. As shown in Appendix B, it can be computed from the perturbative expansion of the RG dimension of the spin variable, obtaining $b_\chi = \pi^2/16$.

We now consider the GRPXY model and study the critical behavior of χ and ξ as one approaches the pure XY critical point along the line $\beta = \beta_{XY} = 1.1199$ by decreasing σ . We collected data for $0.46 \gtrsim \sigma \gtrsim 0.14$ in the infinite-volume limit, corresponding to the quite large range of correlation lengths $4 \lesssim \xi \lesssim 50$. Fig. 4 shows a plot of $\ln \xi$ versus $\sigma^{-1/2}$. The data fall on a straight line, showing that for $\sigma \rightarrow 0$

$$\ln \xi \sim \sigma^{-1/2}. \quad (19)$$

This behavior can be understood within the RG framework. The general discussion presented in Appendix C shows that, as long as disorder is less relevant than the thermal perturbation, the critical behavior can be simply obtained by replacing τ with the nonlinear thermal scaling field. Note that it is not necessary that disorder is irrelevant to obtain the result (19). In general, the thermal nonlinear scaling field u_t is an analytic function of the system parameters. Thus, in the presence of disorder it is a function of

[§] Equation (17) holds whatever the definition of the correlation length is, but of course X depends on the specific choice for ξ . Reference [57] studied the exponential correlation length ξ_{gap} , which is defined as the inverse of the mass gap, and determined the corresponding constant $X_{\text{gap}} = 0.233(3)$. Since in the critical limit [66] $\xi^2/\xi_{\text{gap}}^2 = r = 0.9985(5)$, the constant X for the second-moment correlation length we use is given by $X = X_{\text{gap}}\sqrt{r} = 0.233(3)$.

both $\tau = (T - T_{XY})/T_{XY}$ and σ such that, close to the XY transition point, it behaves as

$$u_t(\tau, \sigma) = \tau + c_\sigma \sigma + \dots \quad (20)$$

where the dots stand for higher-order terms. If disorder is less relevant than the thermal perturbation, then

$$\ln(\xi/X) = C u_t^{-1/2} + O(u_t^{1/2}), \quad (21)$$

along any straight line in the T, σ plane which ends at the XY pure transition point. Since this relation also holds for $\sigma = 0$ and $u_t(\tau, 0) = \tau$, C and X are the same constants reported below (17). Along the line $T = T_{XY}$ Equation (21) implies

$$\ln(\xi/X) = \frac{C}{(c_\sigma \sigma)^{1/2}} + O(\sigma^{1/2}), \quad (22)$$

in agreement with the observed behavior. In order to determine c_σ we have performed fits to

$$\ln(\xi/X) = C_\sigma \sigma^{-1/2} (1 + b\sigma), \quad (23)$$

using $X = 0.233(3)$. We obtain the estimates $C_\sigma = 2.010(2)$ and $b \approx -0.11$. In particular, a fit of the data satisfying $\xi \gtrsim 7$ gives $C_\sigma = 2.0102(8)$ and $b = -0.108(2)$, with $\chi^2/\text{DOF} \approx 1.1$ (DOF is the number of degrees of freedom of the fit). Using $C = 1.776(4)$ and $C_\sigma = C/\sqrt{c_\sigma}$, we obtain

$$c_\sigma = \left(\frac{C}{C_\sigma} \right)^2 = 0.781(4). \quad (24)$$

The constant c_σ is nonuniversal and as such is model dependent. However, for $\sigma \rightarrow 0$ the fields A_{xy} are typically very small and the distribution functions for the GRPXY and CRPXY models are identical to leading order in A_{xy} . We thus expect that the first correction to the thermal scaling field due to disorder is identical in the two models, i.e.

$$u_{t,\text{GRPXY}}(\tau, \sigma) = u_{t,\text{CRPXY}}(\tau, \sigma) + O(\sigma^2), \quad (25)$$

which implies that c_σ is the same in the GRPXY and CRPXY models.

4.2. Critical behavior of the magnetic correlations at fixed σ

Standard arguments that apply to critical lines and multicritical points imply that the critical temperature at fixed σ must be the solution of the equation

$$u_t[T_c(\sigma), \sigma] = 0. \quad (26)$$

Therefore, Equation (20) also implies that for small values of σ the critical temperature for the GRPXY model (and also for the CRPXY model if (25) holds) is given by

$$T_c(\sigma) = T_{XY} [1 - c_\sigma \sigma + O(\sigma^2)]. \quad (27)$$

Equation (27) can be checked by analyzing data at fixed small values of σ . We have performed MC simulations of the GRPXY model at $\sigma = 0.0576$ for several values of β ,

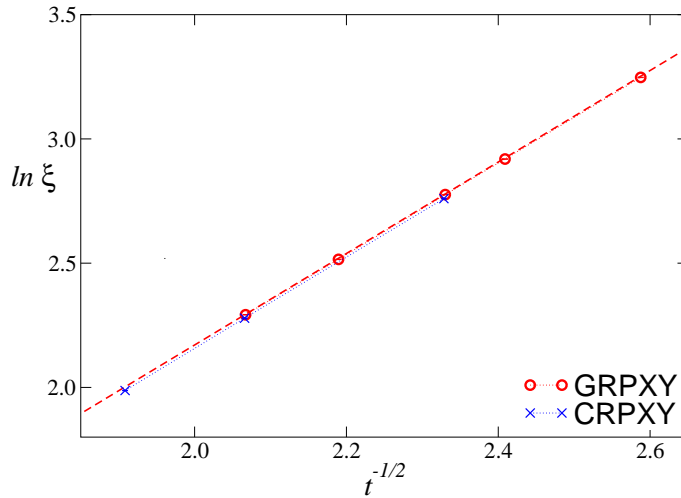


Figure 5. Plots of $\ln \xi$ vs $t^{-1/2}$, where $t \equiv (T - T_c)/T_c$, for the GRPXY and CRPXY models at $\sigma = 0.0576$. For both models we use $T_c = 0.8528$, as obtained by using (27). The dashed line corresponds to a fit of the GRPXY data to $\ln \xi = ct^{-1/2} + a$. The dotted line that connects the MC data is drawn to guide the eye.

from $\beta = 0.95$ to $\beta = 1.02$, corresponding to $10 \lesssim \xi \lesssim 26$, and of the CRPXY model at the same value of σ for $\beta = 0.92, 0.95, 0.99$ corresponding to $7 \lesssim \xi \lesssim 16$. In Fig. 5 we plot ξ versus $t^{-1/2}$ with $t \equiv T/T_c - 1$ and $T_c = 0.8528$ given by (27) [if we take the errors on T_{XY} and c_σ into account, we have $T_c = 0.8528(3)$]. Clearly, $\xi \rightarrow \infty$ as $t \rightarrow 0$, confirming (27). Moreover, they are clearly consistent with the KT behavior

$$\ln \xi = at^{-1/2} + b. \quad (28)$$

A fit of all available data for the GRPXY model to (28) gives $a = 1.841(2)$ and $b = -1.511(5)$ (with $\chi^2/\text{DOF} \approx 1.3$) keeping $T_c = 0.8528$ fixed. A nonlinear fit, taking T_c as a free parameter, gives $T_c = 0.852(2)$, in good agreement with (27). Note that the estimate of the constant b is close to the corresponding XY-model value $\ln X = -1.46(1)$. This is no unexpected since $X(\sigma) = X + O(\sigma)$.

We also collected data at $\sigma = 0.1521$ for both the GRPXY and CRPXY models, for $0.8 \leq \beta \leq 1.1199$ (corresponding to $2 \lesssim \xi \lesssim 37$) and $0.96 \leq \beta \leq 1.145$ (corresponding to $5 \lesssim \xi \lesssim 46$), respectively. Again, the data fit well the KT behavior (28), see Fig. 6. Fits of the MC data for $\xi \gtrsim 10$ to (28) (for which $\chi^2/\text{DOF} < 1$) give the estimates $T_c = 0.772(2)$ for the GRPXY model, and $T_c = 0.762(1)$ for the CRPXY model. Note that (27) would give $T_c = 0.7872$ for $\sigma = 0.1521$, which is slightly larger than the above estimates. This is not unexpected since, when increasing σ , higher-order terms (which are different for the two models) may become important in (20). We also mention the estimates $b = -1.82(7)$ and $b = -1.78(3)$ for the GRPXY and CRPXY model, respectively, from which one obtains estimates of the corresponding length scale $X(\sigma) = e^b$, $X = 0.162(11)$ and $X = 0.169(5)$. We also determined ξ for other values of σ , but in a smaller range. The results are compatible with a KT behavior, but they do not allow us to get robust estimates of T_c . We only mention that in the case of the

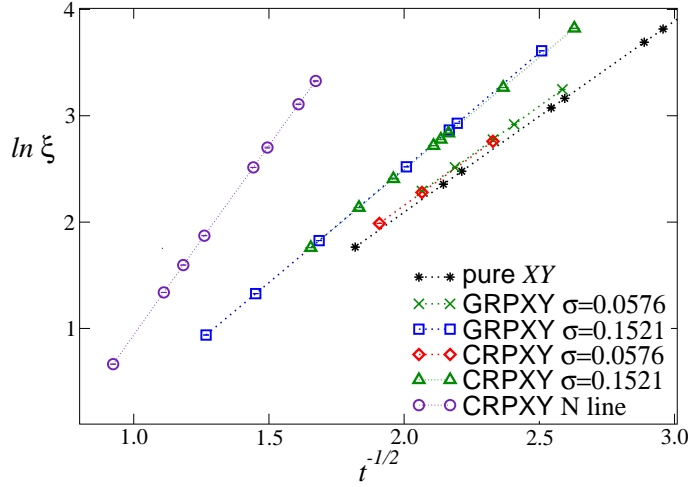


Figure 6. Estimates of $\ln \xi$ vs $t^{-1/2}$, where $t \equiv T/T_c(\sigma) - 1$, for the GRPXY and CRPXY models for several values of σ . For $\sigma = 0.0576$ we take $T_c(\sigma) = 0.8528$ [Equation (27)]. For the other values of σ , $T_c(\sigma)$ is determined from the data. The lines are drawn to guide the eye. The data for the XY are taken from [67].

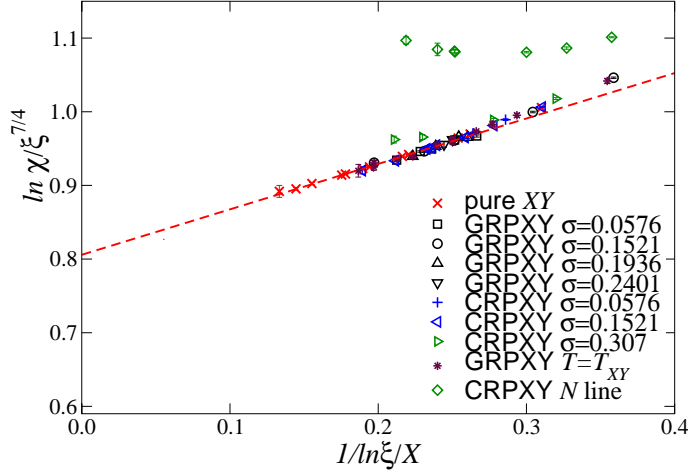


Figure 7. Plot of $\ln(\chi/\xi^{7/4})$ versus $1/\ln \xi/X$. We fix $X = 0.233$, which is the length-scale value valid for the pure XY model. We show data for the pure XY model (taken from [67]), and for the GRPXY and CRPXY models at various values of σ , at $T = T_{XY}$ and along the N line. The dashed line corresponds to a fit to $a + \pi^2/(16 \ln \xi/X)$ of the pure-XY data satisfying $\xi \gtrsim 10$ (we obtain $a = 0.8058(1)$ with $\chi^2/\text{DOF} \approx 0.7$).

GRPXY at $\sigma = 0.1936$, for which we have only data for $\xi \lesssim 20$, we find $T_c \approx 0.74$.

At a KT transition the magnetic susceptibility behaves as in (18), where $b_\chi = \pi^2/16$ is universal. In Fig. 7 we show $\chi/\xi^{7/4}$ for the GRPXY and CRPXY and several values of σ together with those of the pure XY model taken from [67]. We report the data versus $\ln \xi/X(\sigma = 0)$. We could have also used $\ln \xi/X(\sigma)$, where $X(\sigma)$ is determined from the fit of ξ . This choice gives a plot essentially identical to the one reported, which is not unexpected since, by using $\ln \xi/X(\sigma = 0)$ or $\ln \xi/X(\sigma)$ one simply changes the

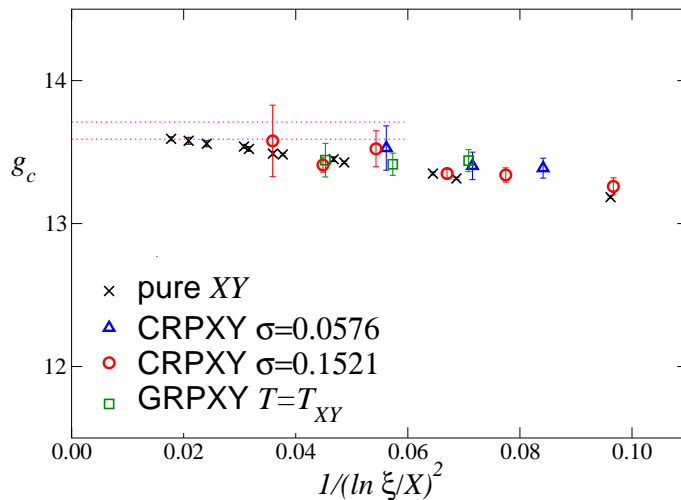


Figure 8. MC estimates of $g_c \equiv g_4 + 3g_{22}$ vs $1/(\ln \xi/X)^2$ with $X = 0.233$. The data for the pure XY model are taken from [67]. The dotted lines correspond to the estimate $g_c^* = g_4^* = 13.65(6)$ obtained by form-factor calculations [67].

corrections of order $\sigma/\ln^2 \xi/X$, which are present anyway. The results appear to follow the same curve within the errors (except those obtained along the N line, which we shall discuss in Sec. 5). They provide strong evidence that the value $\eta = 1/4$ is universal along the thermal paramagnetic-QLRO transition line. Also the slope appears universal (the coefficient b_χ does not depend on σ), as expected on the basis of the discussion of Appendix B. The constant A_χ corresponds to the intercept of $\chi/\xi^{7/4}$ at $\ln \xi/X(\sigma) = 0$. As it can be seen from the figure, this constant, which is not universal, varies very little with σ : differences are not visible within our errors, except for the CRPXY data at $\sigma = 0.307$. However, note that for this value of σ the critical behavior is controlled by the multicritical Nishimori point, i.e. by the special point M which appears in Fig. 1; we will return to it in Sec. 5.

In conclusion, the above numerical results provide a strong evidence that the magnetic two-point correlations show a KT behavior along the thermal paramagnetic-QLRO transition line in GRPXY and CRPXY models.

4.3. Quartic couplings

We now discuss the behavior of the quartic couplings defined in (13)-(15). We recall that in the pure XY model $g_{22} = 0$ while $g_4 = g_c$ behaves as

$$g_4 = g_4^* + \frac{b_g}{(\ln \xi/X)^2} + O(1/\ln^4 \xi), \quad (29)$$

where g_4^* and b_g are universal; see Appendix B. We mention the estimates $g_4^* = 13.65(6)$ obtained by form-factor computations in [67], and $g_4^* = 13.7(2)$ by field-theoretical methods [68]; other results for g_4^* can be found in [69] and references therein.

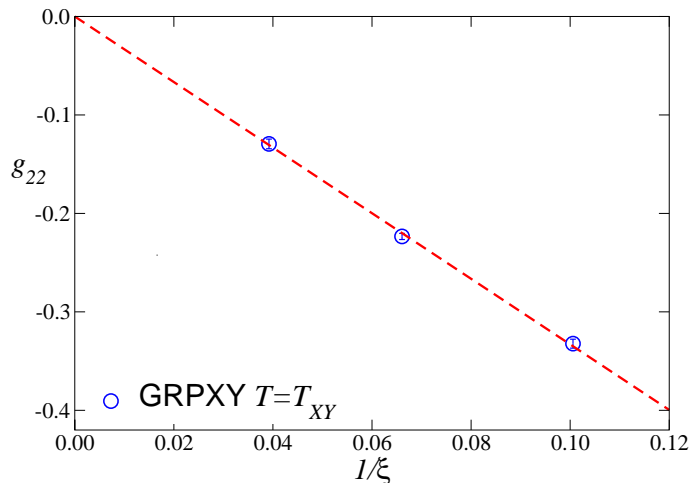


Figure 9. Estimates of g_{22} versus $1/\xi$ for the GRPXY model at fixed $\beta = \beta_{XY} = 1.1199$. The line is a fit of g_{22} to $c\xi^{-1}$.

In Fig. 8 we show some MC results of g_c for the CRPXY model at $\sigma = 0.1521, 0.0576$ and the GRPXY model at $\beta = \beta_{XY} = 1.1199$ (within our errors of a few per mille the infinite-volume limit is reached for $L/\xi \gtrsim 10$, as in the pure XY model [67]), and compare them with MC results for the pure XY model taken from [67]. The results are identical within errors. For example, if we consider the CRPXY model for $\sigma = 0.1521$, a fit to $g_c^* + b_g/(\ln \xi/X)^2$ gives $g_c^* = 13.57(10)$ and $b_g = -3.1(1.4)$, with $\chi^2/\text{DOF} \approx 0.4$, to be compared with the value [67] $g_4^* = 13.65(6)$ of the pure XY model. Both g_c^* and b_g , which are universal in the pure-XY universality class, do not depend on σ .

The quartic coupling g_{22} defined in (14) is interesting because it is particularly sensitive to randomness effects, since in the pure XY model it vanishes trivially. The estimates of g_{22} in the GRPXY model for $T = T_{XY}$ and several values of σ are shown in Fig. 9. They decrease with decreasing σ , and appear to vanish when $\sigma \rightarrow 0$ as

$$g_{22} \sim c\xi^{-\epsilon}, \quad (30)$$

with $\epsilon \approx 1.0$. A fit to (30) gives $\epsilon = 0.97(4)$, $c = 3.1(3)$ with $\chi^2/\text{DOF} \approx 1.1$, where DOF is the number of degrees of freedom of the fit.

The fast decrease of g_{22} along the line $T = T_{XY}$ [note that $g_{22} \sim 1/\xi$ implies $g_{22} \sim \exp(-c\sigma^{-1/2})$] might suggest the irrelevance of disorder, and therefore that the critical value g_{22}^* vanishes along the thermal paramagnetic-QLRO transition line. This conclusion is apparently contradicted by the results at fixed $\sigma > 0$. The results for the CRPXY model at various values of σ , $\sigma = 0.0576, 0.1521, 0.2992, 0.307$, are shown in Fig. 10, where they are plotted versus $(\ln \xi/X)^{-2}$, which is the correction expected in the pure XY model for RG invariant quantities. The coupling g_{22} is quite small, but definitely different from zero on the transition line. For $\sigma = 0.1521$ an extrapolation using $g_{22}^* + b/(\ln \xi/X)^2$ suggests a nonzero critical limit. Using only data satisfying $\xi \gtrsim 10$, this fit gives $g_{22}^* = -0.068(8)$ and $b = -0.080(15)$, with $\chi^2/\text{DOF} \approx 0.4$. We should also mention that the data for the largest values of ξ , those satisfying $\xi \gtrsim 10$ say,

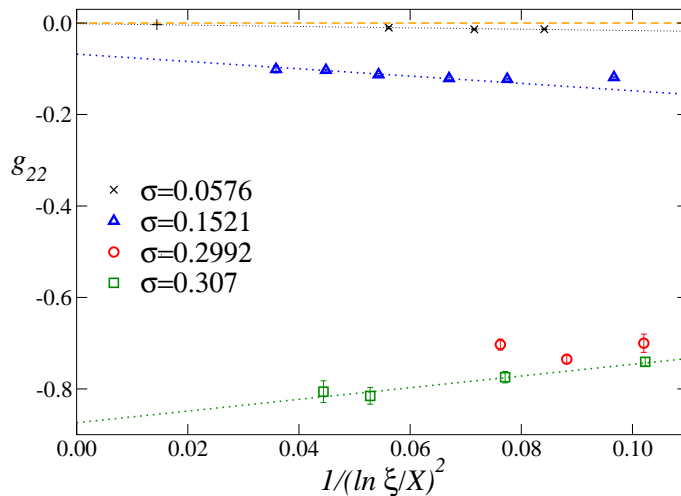


Figure 10. Estimates of g_{22} for the CRPXY model at various values of σ . The lines show linear extrapolations to the critical point. The data denoted by a plus along the line related to $\sigma = 0.0576$ is obtained by using (30) and (23) with the results of the fits along the $T = T_{XY}$ line.

may be consistent with a vanishing critical limit, but only assuming a slower logarithmic approach, i.e., $g_{22} \approx b/(\ln \xi/X)$. For instance, the data with $\xi \gtrsim 10$ are consistent with this behavior (the fit gives $b = -0.482(4)$ with $\chi^2/\text{DOF} \approx 1.1$). At $\sigma = 0.0576$ the $1/(\ln \xi)^2$ extrapolation of the data satisfying $7 \lesssim \xi \lesssim 16$ gives $g_{22}^* = -0.008(6)$ with $\chi^2/\text{DOF} \approx 1.3$. The data of g_{22} at $\sigma \approx 0.30$ are larger, but this can be explained by crossover effects, since this value of σ is quite close to the critical point along the N line, where the critical behavior may change, see Sec. 5.

Overall the results for g_{22} suggest a nonuniversal critical value.

4.4. Critical behavior of the overlap correlations

We now discuss the critical behavior of overlap correlations, cf. (11), which are the appropriate quantities to understand the role of disorder. We consider the critical behavior of the overlap susceptibility which is expected to behave as $\chi_o \sim \xi_o^{2-\eta_o}$. In the case of the pure XY model we have $\eta_o = 2\eta = 1/2$. In [55] it was noted that the following relations

$$2\eta - \eta_o \approx \frac{\sigma}{\pi} \quad \text{for GRPXY,} \quad (31)$$

$$2\eta - \eta_o \approx \frac{\sigma + \frac{1}{2}\sigma^2}{\pi} \quad \text{for CRPXY} \quad (32)$$

approximately hold in the whole QLRO phase (within the small statistical errors), even very close to the KT transition, as long as σ is not too large (in practice σ should not be close to σ_M , where M is the Nishimori point defined in Fig. 1). This would suggest that they may remain valid up to the transition. Given the strong numerical evidence that the exponent η associated with the magnetic correlation is $\eta = 1/4$, see Sec. 4.2,

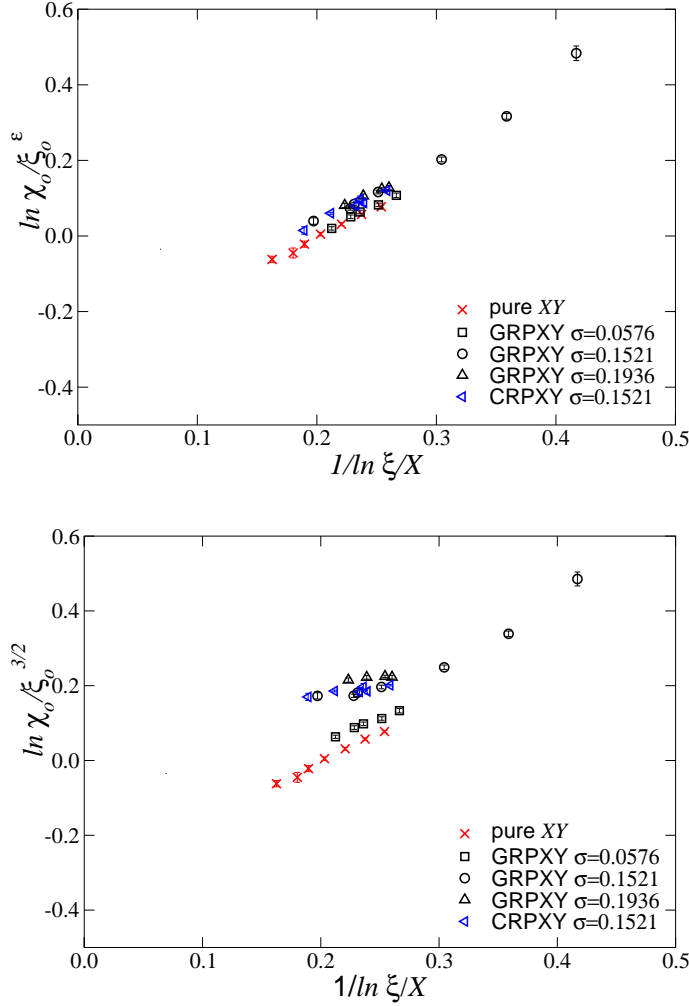


Figure 11. MC estimates of $\chi_o/\xi_o^{\varepsilon(\sigma)}$ (above), where $\varepsilon(\sigma) = 2 - \eta_o(\sigma)$, and $\eta_o(\sigma)$ is given by (33) and (34), and of $\chi_o/\xi_o^{2-\eta_o}$ (below), where we take the pure XY exponent $\eta_o = 1/2$.

the above relations imply that η_o varies along the paramagnetic-QLRO transition line approximately as

$$\eta_o \approx \frac{1}{2} - \frac{\sigma}{\pi} \quad \text{for GRPXY,} \quad (33)$$

$$\eta_o \approx \frac{1}{2} - \frac{\sigma + \sigma^2/2}{\pi} \quad \text{for CRPXY,} \quad (34)$$

at least for sufficiently small values of σ . We wish now to verify if the high-temperature data are consistent with these predictions. In Fig. 11 we plot $\chi_o/\xi_o^{2-\eta_o}$ versus $1/\ln(\xi/X)$. The scaling is reasonable. We also report $\chi_o/\xi_o^{2-\eta_o}$, fixing η_o to the pure XY value $\eta_o = 1/2$. Again the ratio is consistent with a limiting finite value. However, if χ_o behaves as in the pure XY model, we would expect a σ -independent slope, see Appendix B, which is not supported by the data.

We now consider the ratio ξ_o/ξ between the second-moment correlation lengths

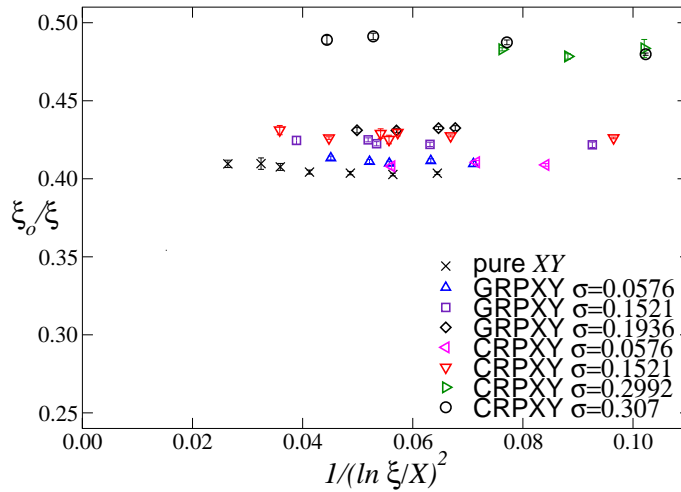


Figure 12. The ratio ξ_o/ξ versus $1/(\ln \xi/X)^2$ for the models considered.

obtained from the overlap and spin correlation functions, cf. (12).^{||} In order to estimate this ratio in the case of the pure XY model, we performed MC simulations (using the cluster algorithm) in the range $0.93 \leq \beta \leq 1.033$ corresponding to $12 \lesssim \xi \lesssim 110$. Taking into account the logarithmic scaling corrections, i.e. fitting the XY-model data satisfying $\xi \gtrsim 32$ to $a + b/(\ln \xi/X)^2$ with $X = 0.233$, we obtain the estimate $\xi_o/\xi = 0.417(4)$. In Fig. 12 we show the results for several values of σ . They are all consistent with a finite critical value, confirming that the paramagnetic-QLRO transitions are characterized by a single diverging length. The results can be extrapolated by assuming $\xi_o/\xi = a + b/(\ln \xi/X)^2$ for $\xi \rightarrow \infty$. We obtain $\xi_o/\xi = 0.417(5)$, $0.428(5)$, $0.425(7)$, $0.425(3)$ for the GRPXY model at $\sigma = 0.0576$, 0.1521 , 0.1936 and the CRPXY model at $\sigma = 0.1521$, respectively. A larger result is found for the CRPXY model at $\sigma \approx 0.299$, 0.307 : $\xi_o/\xi \approx 0.49$.

These results indicate that the ratio ξ_o/ξ varies along the transition line, although it changes very weakly for small values of σ . Again, this is consistent with the observation that disorder-related quantities, like η_o and g_{22} , depend on σ .

5. Critical behavior along the N line in the CRPXY model

We now consider the critical behavior along the N line $T = \sigma$ in the CRPXY model, approaching the transition point from the paramagnetic phase. We recall that along the N line the magnetic and overlap correlation functions are equal, so that $\eta_o = \eta$ and $\xi_o = \xi$ exactly. We performed several MC simulations along the N line, in the range $1.5 \leq \beta \leq 2.4$, corresponding to $2 \lesssim \xi \lesssim 28$, and considered large lattice sizes, in order to obtain infinite-volume results.

Our MC estimates of the magnetic correlation length ξ are consistent with an

^{||} In a Gaussian theory without disorder, in which the magnetic correlation function is given by $\tilde{G}(p) = (p^2 + m^2)^{-1}$, one can easily find that $\xi_o/\xi = \sqrt{1/6} = 0.408248\dots$

exponential increase, i.e. with a behavior of the form $\ln \xi \sim t^{-1/2}$ with $t = T/T_M - 1$, see Fig. 6. A linear fit to

$$\ln \xi = at^{-1/2} + b \quad (35)$$

of the data satisfying $\xi \gtrsim 5$ gives the estimate

$$T_M = \sigma_M = 0.307(2), \quad (36)$$

with $\chi^2/\text{DOF} \lesssim 1.0$. We also mention that alternative fits to $\xi = at^{-b}$ and to $\ln \xi = at^{-1} + b$ give rise to significantly larger χ^2 .

In order to estimate the exponent η , we fit χ and ξ to $\chi = c\xi^{2-\eta}$. Considering the MC results satisfying $\xi \gtrsim \xi_{\min} = 5$, we find $\eta = 0.246(4)$ with $\chi^2/\text{DOF} \approx 1.0$. If we increase ξ_{\min} , η slightly decreases, but it is always compatible with $\eta = 1/4$. These results suggest that $\eta = 1/4$ also along the N line.

Fig. 13 shows the estimates of g_c . The critical limit of g_c is consistent with the results for the pure XY model and those obtained along the thermal paramagnetic-QLRO line at smaller values of σ , see Fig. 8. Indeed, a fit of all data of g_c to (29) gives $g_c^* = 13.49(13)$ with $\chi^2/\text{DOF} \approx 0.6$. If we consider only the data satisfying $\xi \gtrsim 4$, we obtain $g_c^* = 13.6(3)$.

The above-reported results (KT behavior of ξ , $\eta = 1/4$, and $g_c^* \approx g_{4,XY}^*$) suggest that the magnetic correlations behave as in the pure XY model. There is, however, a result which contradicts this hypothesis. As we discussed in Sec. 4.1, the rate of approach of $\chi\xi^{-7/4}$ to its limiting value, should be universal. As can be seen from Fig. 7, this is not the case: the slope of the data along the N line is clearly different from that predicted for the pure XY model. Thus, even though at the Nishimori point the magnetic critical behavior is the same as that observed along the thermal paramagnetic-QLRO transition line, corrections are different, implying the presence of a new (probably marginal) RG operator, which only contributes to scaling corrections in magnetic quantities.

A better evidence for the presence of a new, disorder-related operator is obtained by considering g_{22} and ξ_o/ξ . In Fig. 13 we also report estimates of g_{22} along the N line and along the line $\sigma = 0.307$. If the estimate (36) is correct, the two lines intersect the critical line at the same point, the Nishimori point. It is quite clear from the data that the limiting value of g_{22} along the two lines is quite different. A fit of all available data on the Nishimori line to $g_{22}^* + b/(\ln \xi/X)^2$ gives $g_{22}^* = -7.00(5)$ with $\chi^2/\text{DOF} \approx 0.9$. On the other hand, a fit of the data along the line at fixed $\sigma = 0.307$ gives $g_{22}^* \simeq -0.8$. The same phenomenon is observed for the ratio ξ_o/ξ . As can be seen in Fig. 12, for $\sigma = 0.307$ this ratio is approximately equal to 0.49, which is clearly different from the result that holds exactly along the Nishimori line, $\xi_o/\xi = 1$. The large differences of the values of these two RG invariant quantities along the two lines provide compelling evidence that the Nishimori point is a multicritical point as in the 2D $\pm J$ Ising model [59].

To understand this conclusion, let us review the basic results that apply to multicritical points. The singular part of the free energy should obey a scaling law

$$\mathcal{F}_{\text{sing}}(u_1, u_2) = b^{-d} \mathcal{F}_{\text{sing}}(b^{y_1} u_1, b^{y_2} u_2), \quad (37)$$

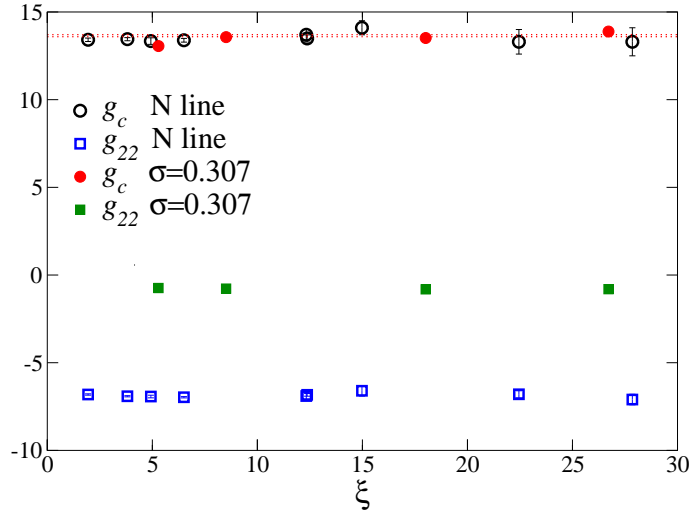


Figure 13. Estimates of g_c and g_{22} along the N line and at $\sigma = 0.307$. The dotted lines indicate the estimate [67] $g_c^* = g_{4,XY}^* = 13.65(6)$ for the pure XY model.

where u_1 and u_2 are two relevant scaling fields. They can be inferred by using the following facts: (i) the transition line at M must be parallel to the T axis, since it has been proved [8] that σ_M is an upper bound for the values of σ where QLRO can exist; (ii) the condition $T = \sigma$ at the N line is RG invariant. We therefore have

$$u_1 = \sigma - \sigma_M + \dots \quad (38)$$

where the dots indicate nonlinear corrections, which are quadratic in $\Delta\sigma \equiv \sigma - \sigma_M$ and $\Delta T \equiv T - T_M$, so that the line $u_1 = 0$ runs parallel to the T axis at M . Moreover, we choose

$$u_2 = T - \sigma, \quad (39)$$

so that the N line corresponds to $u_2 = 0$.

Close to the multicritical point, any RG invariant quantity, such as g_{22} , is expected to behave as

$$R = f_R(u_1 u_2^{-y_1/y_2}). \quad (40)$$

Now, the N-line corresponds to $u_2 = 0$, so that a RG invariant quantity converges to $f_R(\infty)$. On the other hand, the line $\sigma = \sigma_M$ corresponds to $u_1 = 0$, so that a RG invariant quantity converges to $f_R(0)$ which is generically expected to be different from $f_R(\infty)$. Thus, if the Nishimori point is multicritical, we expect RG invariant quantities to have a different critical value along the two lines. This is exactly what we observe for g_{22} and ξ_o/ξ . Thus, in view of the numerical results we conclude that the Nishimori point is a multicritical point.

It is interesting to note that the multicritical behavior is not observed in the magnetic sector. For instance, g_c^* along the paramagnetic-QLRO line is equal to its

XY value $g_{4,XY}^*$. The same result holds along the Nishimori line. In terms of the scaling function f_{g_c} defined in (40) these results imply

$$f_{g_c}(0) = f_{g_c}(\infty) = g_{4,XY}^* . \quad (41)$$

It is then natural to conjecture that $g_c^* = g_{4,XY}^*$ along any line that intersects the Nishimori point, i.e. that $f_{g_c}(x) = g_{4,XY}^*$ for any x . The absence of multicritical behavior in the magnetic sector is also supported by the fact that ξ always shows a KT behavior and that the magnetic exponent η at the Nishimori point is equal to the pure-XY value $1/4$.

The results we have presented should apply to generic RPXY model. In all cases we expect a multicritical point along the paramagnetic-QLRO transition line. It follows from universality that, at the multicritical point, the magnetic and the overlap correlation functions have the same critical behavior—hence, we have $\eta = \eta_o$ —though they may not be necessarily equal as is the case for the CRPXY model. Note that this point is not expected in general to coincide with that in which the tangent to the transition line is parallel to the T axis.

6. Glassy critical behavior at $T = 0$

In the limit $\sigma \rightarrow \infty$ the RPXY model corresponds to the gauge-glass model in which the phase shifts are uniformly distributed. This model has been extensively studied both at zero and at finite temperature [5, 10, 14, 15, 16, 17, 18, 19, 21, 22, 25, 26, 29, 32, 33, 34, 36, 38, 40, 41, 43, 44, 45, 46, 47, 48, 49, 50, 51, 52, 53, 54]. [21, 22] showed that no long-range glassy order can exist at finite temperature. Although this result does not exclude the possibility of a finite-temperature transition with an exotic low-temperature glassy phase, for example a phase characterized by glassy QLRO, most numerical works [5, 19, 36, 43, 45, 46, 49, 50, 51] support a zero-temperature glassy critical behavior. The overlap correlation length ξ_o diverges as $T^{-\nu}$ for $T \rightarrow 0$. We mention the estimates [45] $1/\nu = 0.39(3)$ and [49] $1/\nu = 0.36(3)$ from finite-temperature MC simulations, and [43] $1/\nu = 0.36(1)$ and [51] $1/\nu \approx 0.45$ from $T = 0$ numerical calculations. Moreover, if one assumes that the ground state is nondegenerate in the overlap variables, one obtains that at $T = 0$ the finite-size overlap susceptibility satisfies the relation $\chi_o = L^2$, so that $\eta_o = 0$. We mention that this scenario was questioned in [41, 40, 44, 47, 48, 52, 53, 54], which claimed the existence of a finite-temperature transition at $T \approx 0.2$.

A natural scenario for the phase digram of the GRPXY and CRPXY models is that the glassy transition, which occurs for $\sigma = \infty$, is not isolated but that it is the endpoint of a phase transition line that starts at the paramagnetic-QLRO transition line. In particular, if the zero-temperature glassy transition scenario applies to the gauge-glass model, we expect a line of $T = 0$ glassy transitions for any $\sigma > \sigma_D$, see Fig. 1. A natural conjecture would be that all these transitions belong to the same universality class.

To check this scenario we performed MC simulations of the CRPXY model at $\sigma = 2/3, 5/9, 1/2, \infty$, which are larger than $\sigma_D \leq \sigma_M \approx 0.31$. As we shall see, the

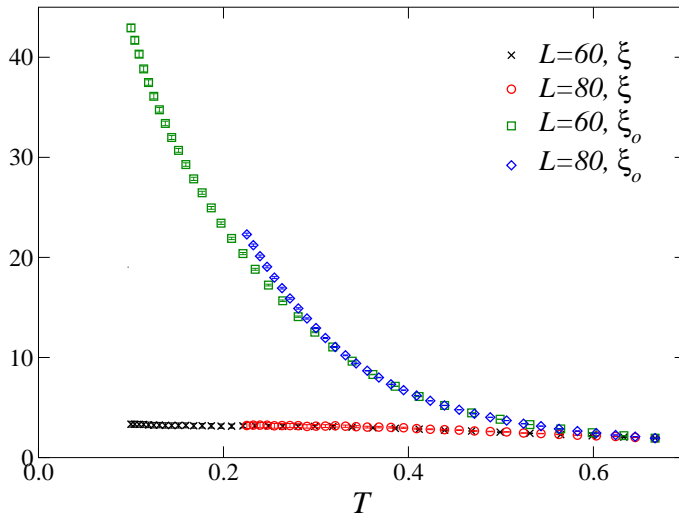


Figure 14. MC estimates of the correlation lengths ξ and ξ_o for the CRPXY model at $\sigma = 2/3$.

results clearly support a glassy $T = 0$ transition in the same universality class as that of the gauge-glass model.

6.1. MC simulations

We performed MC simulations of the CRPXY model on square $L \times L$ lattices with periodic boundary conditions. Most of the results we shall present refer to runs with $\sigma = 2/3$. In this case we considered $L = 20, 30, 40, 60, 80$ and temperatures between $T = 2/3$ (at the Nishimori line) and $T = 0.1$ (for $L = 80$ we considered $0.22 \leq T \leq 2/3$). We averaged over a relatively large number N_s of samples: $N_s = 6000, 9000, 7000, 3000$, and 2000 samples for $L = 20, 30, 40, 60$ and 80 , respectively. We used the MC algorithm discussed in Appendix A combined with the parallel-tempering method [70, 71]. Moreover, to check the universality of the transitions, we also performed parallel-tempering MC simulations for $\sigma = 5/9$ and lattice sizes $L = 60, 70$ (5000 and 1000 disorder samples, respectively), $\sigma = 1/2$ and $L = 70$ (1000 samples), and $\sigma = \infty$ and $L = 20, 30, 40, 60$ (5000, 5000, 2000, 2000 samples, respectively). The points in the T - σ plane where we collected MC data are shown in Fig. 3.

At the glassy transition the critical modes are those related to the overlap variables, while the magnetic ones are noncritical. This is clearly shown in Fig. 14, which shows ξ and ξ_o for $\sigma = 2/3$. The overlap correlation length ξ_o increases steadily with decreasing the temperature, while the magnetic correlation length ξ freezes at sufficiently low temperatures at a value $\xi \approx 3.3$. Therefore, the critical temperature and exponents must be determined from quantities related to the overlap correlation functions.

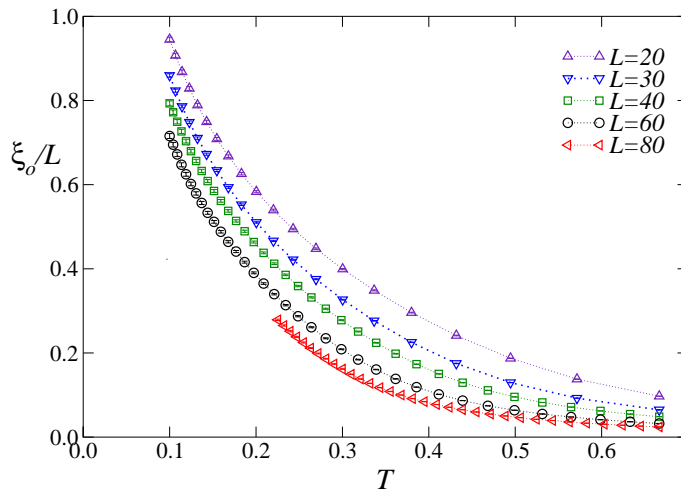


Figure 15. MC estimates of the ratio $R_{\xi_o} \equiv \xi_o/L$ for the CRPXY model at $\sigma = 2/3$.

L_{\min}	T_{\max}	χ^2/DOF	T_c
20	0.6	169/157	0.018(1)
20	0.5	99/141	0.009(1)
20	0.4	67/119	0.010(2)
20	0.3	30/92	0.010(3)
30	0.6	137/138	0.017(1)
30	0.5	66/123	0.008(2)
30	0.4	49/103	0.007(3)
30	0.3	21/79	0.005(4)
40	0.6	106/119	0.017(2)
40	0.5	42/105	0.007(2)
40	0.4	31/87	0.007(3)
40	0.3	17/66	0.007(5)

Table 1. Estimates of T_c obtained by fitting R_{ξ} to (42) with $n = 6$. DOF is the number of degrees of freedom of the fit.

6.2. Evidence for a $T = 0$ glassy transition at $\sigma = 2/3$

In order to determine the critical temperature, we analyze $R_{\xi_o} \equiv \xi_o/L$. The results, shown in Fig. 15, show no evidence of a crossing point in the range of values of T of the data, $T \geq 0.1$, and thus provide the bound $T_c < 0.1$ for the critical temperature T_c . A more precise determination of T_c can be obtained by a finite-size scaling (FSS) analysis. We fit the data to

$$R_{\xi_o} = P_n[(T - T_c)L^{1/\nu}], \quad (42)$$

keeping T_c and ν as free parameters. Here $P_n(x)$ is a polynomial in x of order n . The order n is fixed by looking at the χ^2 of the fit. For each n we determine the goodness $\chi^2(n)$ of the fit. Then, we fix n such that $\chi^2(n)$ is not significantly different from $\chi^2(n+1)$. The results we report correspond to $n = 6$. To identify the role of the corrections to scaling we repeat the fit several times. Each time we fix two parameters

L_{\min}	T_{\max}	χ^2/DOF	ν
20	0.4	100/120	2.465(6)
20	0.3	44/93	2.496(10)
20	0.25	24/77	2.528(14)
20	0.2	17/55	2.547(22)
20	0.16	14/39	2.548(31)
30	0.4	55/104	2.446(6)
30	0.3	23/80	2.464(13)
30	0.25	13/65	2.489(20)
30	0.2	10/46	2.492(30)
30	0.16	9/32	2.488(42)
40	0.4	36/88	2.432(7)
40	0.3	19/67	2.451(15)
40	0.25	12/53	2.480(26)
40	0.2	8/37	2.490(38)
40	0.16	9/25	2.482(53)

Table 2. Estimates of ν obtained by fitting R_{ξ_σ} to (42) with $T_c = 0$ and $n = 6$. DOF is the number of degrees of freedom of the fit.

T_{\max} and L_{\min} and we only include the data which correspond to lattices satisfying the conditions $T \leq T_{\max}$ and $L \geq L_{\min}$.

In Table 1 we report the estimates of T_c for several values of T_{\max} and L_{\min} . We obtain estimates of T_c which are quite small and satisfy the upper bound

$$T_c \lesssim 0.01 . \quad (43)$$

Since our data satisfy $T \geq 0.1$, this estimate allows us to conclude that our results are fully consistent with a zero-temperature transition. From now on, we always assume $T_c = 0$.

6.3. The critical exponent ν

In order to determine the critical exponent ν related to the divergence of the correlation length ξ_σ , we repeat the fit (42) at $\sigma = 2/3$ setting $T_c = 0$. The results are reported in Table 2. They slightly increase as T_{\max} or L_{\min} is lowered, but these changes are small compared to the statistical errors.

In fit (42) we made two approximations. First, we neglected the nonanalytic scaling corrections, which decrease as $L^{-\omega}$. The results indicate that these corrections are small: at fixed $T_{\max} < 0.25$ the estimates of ν obtained setting $L_{\min} = 30$ and $L_{\min} = 40$ differ by much less than the statistical errors. Second, we approximated the thermal nonlinear scaling field u_T by $u_T \approx T$, neglecting the *analytic* corrections (see [72] for an extensive discussion of this type of corrections). To understand their quantitative role, we performed fits to

$$R_\xi = P_n(u_T L^{1/\nu}), \quad u_T \equiv T + pT^2, \quad (44)$$

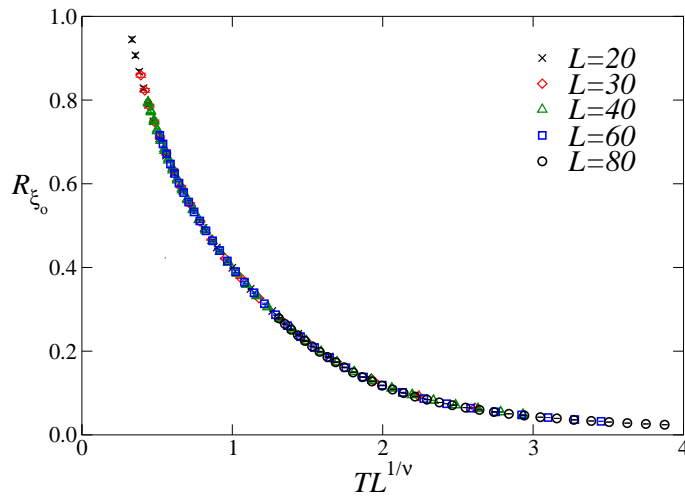


Figure 16. $R_{\xi_o} \equiv \xi_o/L$ versus $TL^{1/\nu}$ for $\nu = 2.5$. Data corresponding to $\sigma = 2/3$.

L_{\min}	T_{\max}	χ^2/DOF	ν	p
20	0.5	98/141	2.54(1)	-0.11(1)
20	0.4	63/119	2.62(2)	-0.20(2)
20	0.3	28/92	2.71(4)	-0.34(5)
20	0.25	20/76	2.67(6)	-0.26(11)
20	0.2	16/54	2.67(10)	-0.29(21)
30	0.5	89/123	2.42(2)	-0.00(2)
30	0.4	47/103	2.54(2)	-0.12(3)
30	0.3	20/79	2.58(5)	-0.18(7)
30	0.25	13/64	2.54(7)	-0.11(14)
30	0.2	10/45	2.50(12)	-0.01(31)
40	0.5	50/105	2.42(2)	-0.00(2)
40	0.4	31/87	2.50(3)	-0.09(3)
40	0.3	17/66	2.58(6)	-0.20(7)
40	0.25	12/52	2.54(16)	-0.12(16)
40	0.2	10/36	2.50(13)	-0.01(33)

Table 3. Estimates of ν and p obtained by fitting R_{ξ_o} to (44) with $n = 6$. DOF is the number of degrees of freedom of the fit.

where p is a new free parameter. The results are reported in Table 3. Corrections are tiny and we estimate $|p| \lesssim 0.2$, so that $|u_T - T|/T$ is at most 0.10, 0.02 for $T = 0.5$, 0.1, respectively. The estimates of ν do not vary significantly and, for $L \geq 30$ and $T_{\max} \leq 0.2$, are fully consistent with those obtained before. We quote

$$\nu = 2.5(1) , \quad 1/\nu = 0.40(2) \quad (45)$$

as our final estimate.

To show the quality of our FSS results in Fig. 16 we plot R_{ξ} versus $TL^{1/\nu}$, using the estimate (45). All data fall on top of each other with remarkable precision.

L_{\min}	T_{\max}	Fit (48)		Fit (49)	
		χ^2/DOF	η	χ^2/DOF	η
20	0.5	11570/142	0.13(2)	338/140	-0.01(1)
20	0.4	1439/120	0.10(2)	99/118	0.02(1)
20	0.3	498/93	0.06(1)	39/91	0.04(3)
20	0.25	182/77	0.06(1)	20/75	0.01(3)
20	0.2	43/55	0.05(1)	12/53	-0.04(8)
30	0.5	6592/124	0.17(2)	263/122	-0.03(2)
30	0.4	1096/104	0.11(2)	78/102	0.01(2)
30	0.3	330/80	0.07(1)	35/78	0.04(3)
30	0.25	89/65	0.05(1)	18/63	0.00(4)
30	0.2	28/46	0.05(2)	11/44	-0.06(10)
40	0.5	4237/106	0.18(2)	177/104	-0.05(2)
40	0.4	1096/88	0.11(2)	40/86	-0.03(2)
40	0.3	294/67	0.07(1)	22/65	0.02(4)
40	0.25	63/53	0.05(1)	9/51	-0.02(6)
40	0.2	17/37	0.04(1)	2/35	-0.11(12)

Table 4. Estimates of η . On the left we report the results of the fits to (48) with $n = 6$, on the right those to (49) with $n = 6$ and $m = 2$. In both cases we fix $\nu = 2.5(1)$. The reported errors are the sum of the statistical error and of the variation of the estimate of η as ν changes by one error bar. DOF is the number of degrees of freedom of the fit.

6.4. The critical exponent η_o

As discussed at length in [72], the overlap susceptibility behaves in the critical limit as

$$\chi_o = \bar{u}_h^2 L^{2-\eta_o} f(u_T L^{1/\nu}). \quad (46)$$

Here u_T is the temperature nonlinear scaling field, while \bar{u}_h is related to the external *overlap-magnetic* scaling field u_h associated with the overlap variables by $u_h = h\bar{u}_h(T) + O(h^2)$. We have already checked that the thermal scaling field u_T can be effectively approximated by $u_T = T$. Thus, neglecting nonanalytic scaling corrections, the data should behave as

$$\ln \chi_o = (2 - \eta_o) \ln L + \ln \bar{u}_h(T)^2 + \ln f(TL^{1/\nu}). \quad (47)$$

We now estimate η_o from the analysis of the data at $\sigma = 2/3$. In a first set of fits we set $\bar{u}_h = 1$ and approximate $\ln f(x)$ with a polynomial in x of order n , i.e., we perform fits to

$$\ln \chi_o = (2 - \eta) \ln L + P_n(TL^{1/\nu}). \quad (48)$$

The analysis of the χ^2 of the fits indicate that $n = 6$ allows us to describe accurately the data. We fix ν to the estimate (45) to avoid an additional nonlinear parameter in the fit. The results are reported in Table 4. We observe a significant change of the estimates as T_{\max} decreases; moreover, the quality of the fit is quite poor. This can be explained by the presence of sizeable analytic corrections, which means that \bar{u}_h is poorly approximated by a $\bar{u}_h = 1$ in our range of temperatures. The same phenomenon occurs

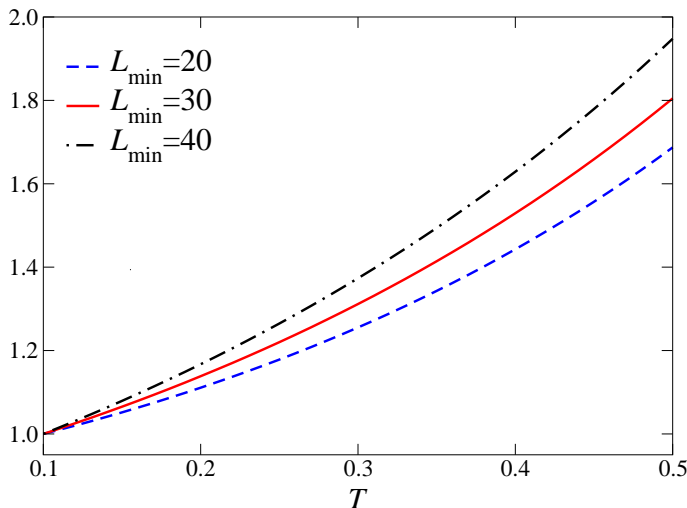


Figure 17. Plot of the ratio $\bar{u}_h(T)/\bar{u}_h(T = 0.1)$ from fits with $T_{\max} = 0.5$ and $L_{\min} = 20, 30, 40$.

in the three-dimensional Ising spin glass [72], where the analytic corrections cannot be neglected in the analysis of the overlap susceptibility. We thus perform a second set of fits in which we take into account the magnetic nonlinear scaling field. If we approximate $\ln \bar{u}_h^2$ with a polynomial of order m , we end up with the fitting form

$$\ln \chi_o = (2 - \eta) \ln L + P_n(TL^{1/\nu}) + Q_m(T) , \quad (49)$$

where we assume $Q_m(0) = 0$. In the following we take $m = 2$ and again fix ν to the estimate (45). The results are reported in Table 4. The quality of the fit is now significantly better, indicating that the analytic corrections are important. The scaling function \bar{u}_h is reported in Fig. 17 and indeed it varies significantly in the range of values of T we are considering. The estimates of η_o do not show any systematic variation with T_{\max} and are always consistent, within errors, with $\eta_o = 0$. Quantitatively, our data allow us to set the upper bound

$$|\eta_o| \leq 0.05. \quad (50)$$

6.5. Results for the gauge-glass model

In order to check universality we also performed runs at $\sigma = \infty$, although in this case we considered smaller lattices and the errors are significantly larger (partly because of the smaller number of samples, partly because of larger sample-to-sample fluctuations). The data were analyzed as we did in the $\sigma = 2/3$ case. First, we determined the critical temperature T_c . A fit of ξ_o/L to (42) gives rather small estimates of T_c . For $L_{\min} = 20$ we obtain $T_c = 0.030(2)$ [0.020(3)] for $T_{\max} = 0.4$ (resp. 0.3). Thus, we can conclude that $T_c \lesssim 0.02$, which is clearly consistent with $T_c = 0$, given that our data belong to the range $T \geq 0.1$. The claim that $T_c \approx 0.2$ is not consistent with our MC data.

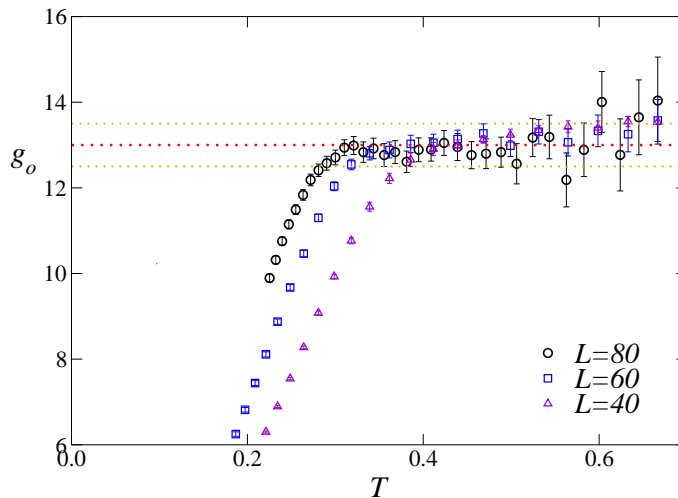


Figure 18. MC estimates of g_o vs T at $\sigma = 2/3$ for $L = 40, 60, 80$. The dotted lines correspond to the infinite-volume critical ($T = 0$) estimate $g_o^* = 13.0(5)$.

Then, we determined ν by assuming $T_c = 0$. The results of the fits to (42) show a significant dependence on T_{\max} . For $L_{\min} = 20$, ν varies between 2.50(1) and 2.80(4) as T_{\max} varies between 0.4 and 0.16. If analytic scaling corrections are included, i.e. we fit the data to (44), we observe a significantly smaller dependence on T_{\max} , but, on the other hand, a rather large dependence on L_{\min} , with rapidly increasing error bars as L_{\min} increases. This is probably due to the fact that we have a somewhat large statistical error on the results with the largest value of L , $L = 60$. The estimates of ν vary between 2.8 and 3.7 if we take $L_{\min} = 20, 30$ and $0.2 \leq T_{\max} \leq 0.5$ and thus give the final result $\nu = 3.3(5)$. This result is somewhat larger than the estimate (45), but certainly not inconsistent. It supports — very weakly, though—universality. A better check is presented below.

6.6. The quartic coupling g_o and universality

We computed the overlap quartic coupling g_o defined in (16). MC results at $\sigma = 2/3$ are shown in Fig. 18. The infinite-volume limit, within our statistical accuracy, is apparently reached when $L/\xi_o \gtrsim 7$, corresponding to $T \gtrsim 0.3$ for our largest lattices $L = 60, 80$. The infinite-volume results are quite stable with respect to T , so that we can reliably estimate the critical ($T = 0$) value g_o^* . We obtain

$$g_o^* = 13.0(5). \quad (51)$$

According to standard RG arguments, g_o has a universal FSS limit as a function of $R_{\xi_o} \equiv \xi_o/L$, that is

$$g_o(T, L) = f(R_{\xi_o}), \quad (52)$$

where the function $f(x)$ is universal and satisfies $f(0) = g_o^*$. This scaling behavior is nicely supported by the data at $\sigma = 2/3$ for various lattice sizes, see Fig. 19. Universality

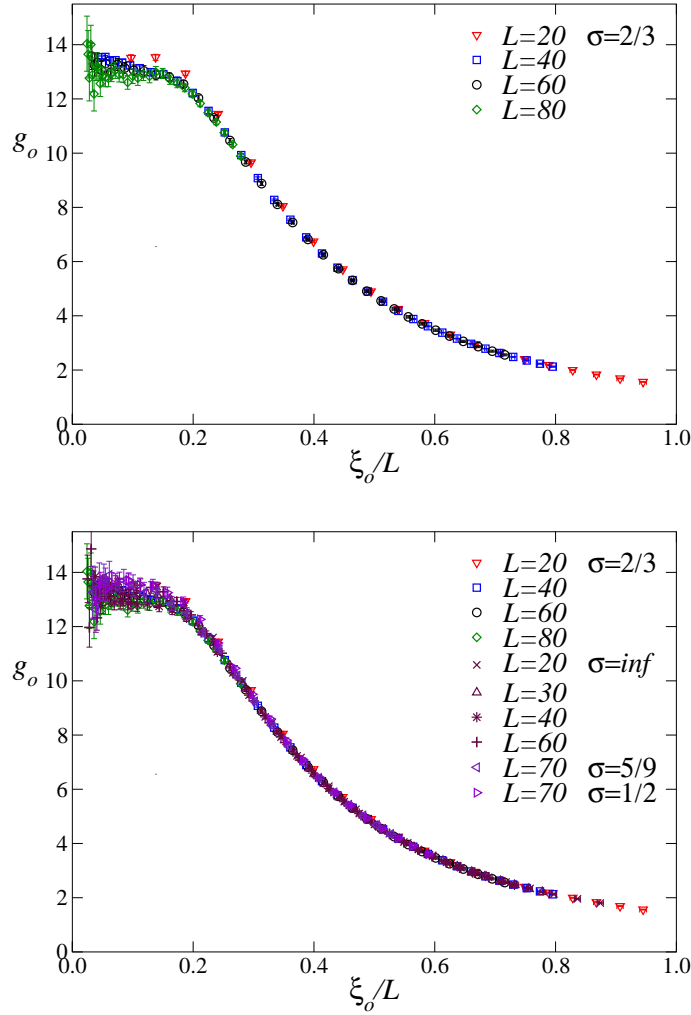


Figure 19. g_o vs $R_{\xi_o} \equiv \xi_o/L$: data at $\sigma = 2/3$ for various lattice sizes $L = 20, 40, 60, 80$ (above), and including (below) also data for other values of σ : $\sigma = 5/9, 1/2, \infty$.

can be checked by also considering the results for $\sigma = 5/9$, $\sigma = 1/2$ and $\sigma = \infty$. Clearly, all points fall on top of each other. Note that here there are no free parameters to fiddle with and thus this comparison provides strong support to the hypothesis that all these models belong to the same universality class. Given the very good evidence we have that the model with $\sigma = 2/3$ undergoes a $T = 0$ glassy transitions, this result further confirms (and provides stronger evidence than that given in the previous paragraph) that the gauge-glass model does not have a finite-temperature exotic glassy transition.

6.7. Behavior of the magnetic correlation functions

Let us now consider the magnetic quantities. The magnetic correlation length ξ is zero in the gauge-glass model, see Appendix E, and increases as one approaches the QLRO region. In particular, at $T = 0.159$, which is below the critical temperature $T_M \approx 0.31$

along the Nishimori line, we obtain $\xi = 3.3(1), 6.7(4), 9.8(3)$ at $\sigma = 2/3, 5/9, 1/2$, respectively. They are roughly consistent with a behavior like $\ln \xi \sim (\sigma - \sigma_c)^{-\kappa}$ assuming $\sigma_c \approx \sigma_M \approx 0.30$, i.e., with a KT-like behavior along the transition line that connects the Nishimori critical point M , see Fig. 1, and the $T = 0$ transition point at $\sigma = \sigma_D$, which is expected to run almost parallel to the T axis. Note, however, that while our data suggest a power-law divergence of $\ln \xi$ (therefore, ξ has an exponential divergence), they are not sufficiently precise to allow us to estimate the power κ . The KT value $\kappa = 1/2$ is consistent with the data, but $\kappa = 1$ would be equally reasonable.

It is also interesting to discuss the behavior of the quartic couplings g_c, g_4 , and g_{22} defined from the magnetic correlation functions in (13)-(15). In Appendix E, assuming universality, we predict that, in the critical limit, g_4 and g_{22} should diverge as ξ_o^2 , while $g_c \xi_o^{-2}$ should go to zero.

Numerical estimates of g_c are shown in Fig. 20. The results are clearly consistent with a finite $T = 0$ limit. Note that the estimates obtained for $\sigma = 2/3, 5/9$, and $1/2$ are close to the XY value $g_{4,XY}^* = 13.65(6)$; actually, they are consistent within errors, even at small T , below $T_M \approx 0.31$. These results are suggestive of a KT behavior of the magnetic correlation functions also along the disorder paramagnetic-QLRO transition line from M to D , see Fig. 1. Indeed, for $\sigma = 2/3, 5/9, 1/2$ we have $\xi \approx 3, 7, 10$, so that along these lines one should be able to observe the critical behavior that arises when one approaches the paramagnetic-QLRO transition line at a point with $T < T_M$. In other words, these results imply that the critical limit of $g_c(\sigma, T)$ at fixed $T < T_M$ along the paramagnetic-QLRO transition line is consistent with the KT value. This fact provides some evidence that also along the disorder-driven transition line magnetic correlation functions behave as in the pure XY model. Of course, as σ increases (thus, the magnetic correlation length ξ decreases), g_c changes significantly and, for $\sigma = \infty$, g_c is infinite for any T and L .

The couplings g_{22} and g_4 are instead expected to diverge as ξ_o^2 . In Fig. 21 we report g_{22} for the different models. The data are clearly diverging as $\xi \rightarrow \infty$, but the asymptotic behavior $g_{22} \sim \xi_o^2$ is not clearly observed, likely because the values of ξ_o are not sufficiently large. Indeed, we only observe that g_{22} behaves as ξ_o^κ with κ rapidly increasing with ξ_o . More precisely, if we only include data satisfying $\xi_o \lesssim 10$ we obtain $\kappa \approx 1$. If instead we fit the data with $10 \lesssim \xi_o \lesssim 20$ (we have infinite-volume data only up to $\xi_o \approx 20$) we obtain $\kappa \approx 1.5$.

7. Conclusions

We have studied the magnetic and glassy transitions of the square-lattice XY model in the presence of random phase shifts and, in particular, the GRPXY and CRPXY model defined by the distributions (2) and (3). The latter is very useful because it allows some exact calculations along the Nishimori line $T = \sigma$ [8, 9], where, in particular, the magnetic and overlap two-point functions are equal. We present MC for the GRPXY and CRPXY models for several values of the temperature and of the parameter σ controlling

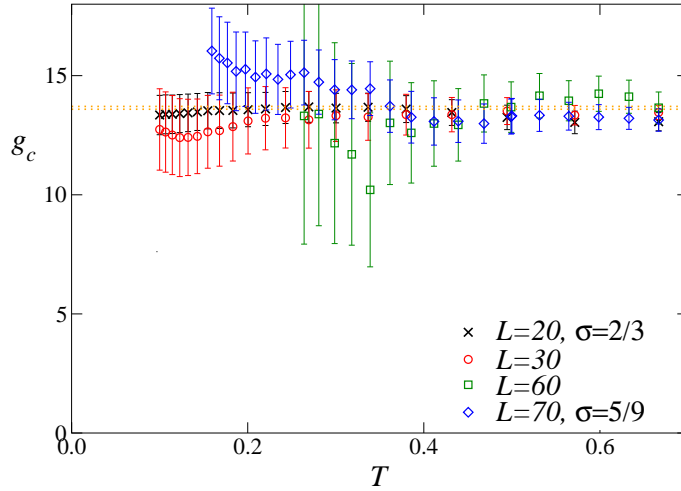


Figure 20. MC estimates of the quartic couplings g_c . The dotted line corresponds to the XY value $g_c = g_4 = 13.65(6)$.

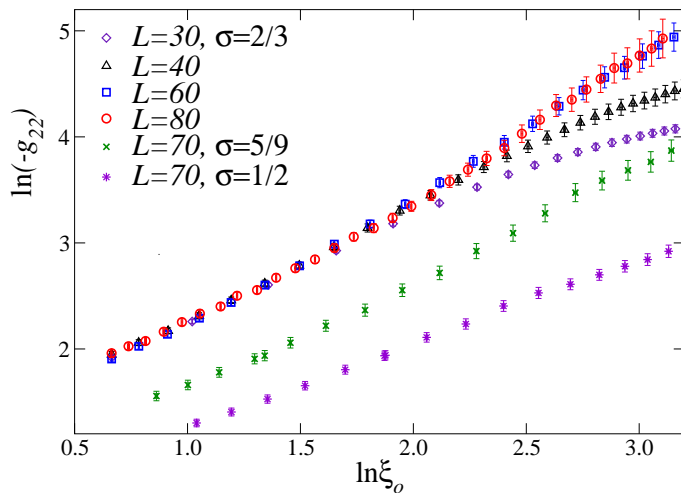


Figure 21. Plot of $\ln(-g_{22})$ vs $\ln \xi_o$ at $\sigma = 2/3, 5/9, 1/2$.

the disorder, approaching the magnetic and glassy transition lines from the paramagnetic phase. We substantially confirm the phase diagram shown in Fig. 1.

Our main results are the following.

- (i) We have carefully investigated the critical behavior along the transition line separating the paramagnetic and QLRO phases, from the pure XY point P to the multicritical point, which, in the CRPXY model, lies on the N line and is such that the transition line runs parallel to the T axis. The magnetic observables show a σ -independent KT behavior: the magnetic correlation length behaves as $\ln \xi \sim u_t^{-1/2}$, where u_t is the thermal scaling field, $u_t \sim T - T_c(\sigma)$, and the magnetic susceptibility as $\chi \sim \xi^{7/4}$ (corresponding to $\eta = 1/4$). Moreover, the quartic coupling g_c defined in (15) appears to be universal. We obtain $g_c^* \approx 13.6$, which is nicely consistent

with the corresponding value $g_{4,XY}^* = 13.65(6)$ of the pure XY model [67, 69]. We have also verified the universality of the leading logarithmic correction to the critical behavior of χ . On the other hand, the critical behavior of disorder-related quantities, such as those related to the overlap correlation function, depends on σ .

- (ii) In the CRPXY model, the Nishimori point M , see Fig. 1, is a multicritical point which divides the paramagnetic-QLRO line into two parts: a thermally-driven transition line (from P to M) and a disorder-driven transition line (from M to D). This result should be general: a multicritical point should also exist in generic RPXY models, although in this case it is not expected to coincide with that where the transition line runs parallel to the T axis. Such a multicritical point is characterized by the fact that, at criticality, magnetic and overlap functions have the same critical behavior, that is $\eta = \eta_o$: in the CRPXY model the two correlation functions are exactly equal (more generally, they are equal on the whole N line), but we do not expect this property to be generic. It is interesting to observe that the multicritical behavior is only observed in the disorder-related quantities. Magnetic observables behave, as far as the leading behavior is concerned, as in the pure XY model: the correlation length shows a KT behavior, $\eta = 1/4$, and $g_c^* = g_{4,XY}^*$ in the whole neighborhood of the multicritical point. However, corrections are different from those appearing in the pure XY model, providing additional evidence for the presence of an additional (probably marginal) RG operator, which is responsible for the multicritical behavior.
- (iii) Little is known about the behavior along the transition line from the multicritical point to D . However, the fact that purely magnetic observables behave as in the pure XY model both along the thermally-driven transition line and at the multicritical point make us conjecture that the magnetic behavior is also unchanged. We have presented some very weak evidence in Sec. 6.7.
- (iv) We have investigated the critical behavior for large values of σ . We find no evidence of a finite-temperature transition for all values of σ we have investigated: the system is paramagnetic up to $T = 0$, where a glassy transition occurs. Moreover, in all cases we verify universality. We can thus conjecture that the critical behavior along the whole line that starts in D , see Fig. 1, is universal: for any $\sigma > \sigma_D$, one has the same critical behavior characterized by the exponents:

$$\nu = 2.5(1), \quad 1/\nu = 0.40(2), \quad |\eta_o| \leq 0.05. \quad (53)$$

Our estimate of ν is consistent with earlier estimates obtained by MC simulations of the gauge-glass XY model, for examples $1/\nu = 0.39(3)$ and $1/\nu = 0.36(3)$ obtained in [45] and [49] respectively, and by numerical calculations of the stiffness exponent at $T = 0$, for example $1/\nu = 0.36(1)$ and $1/\nu \approx 0.45$ obtained in [45] and [51]. Our result for η_o is consistent with a general argument which predicts $\eta_o = 0$.

Appendix A. Details on the Monte Carlo simulation

In the simulation we use both Metropolis and microcanonical local updates. The latter do not change the energy of the configuration and are defined as follows. Consider a site i ; the corresponding field is ψ_i . The terms of the Hamiltonian that depend on ψ_i can be written as

$$\mathcal{H}_i = \text{Re}(\bar{\psi}_i z), \quad z \equiv \sum_j U_{ij} \psi_j, \quad (\text{A.1})$$

where the sum is over all nearest neighbors j of site i . Then, define

$$\psi'_i = 2 \frac{z}{|z|^2} \text{Re}(\bar{\psi}_i z) - \psi_i \quad (\text{A.2})$$

One can verify that $|\psi'_i| = 1$ and that

$$\text{Re}(\bar{\psi}_i z) = \text{Re}(\bar{\psi}'_i z). \quad (\text{A.3})$$

Thus, the update $\psi_i \rightarrow \psi'_i$ does not change the energy and can therefore be always accepted. This update does not suffer the limitations of the Metropolis update: ψ_i and ψ'_i are not close to each other.

In our simulation a MC step consists of 5 microcanonical sweeps over all the lattice followed by one Metropolis sweep. For each disorder sample we typically perform $O(10^5)$ MC steps. In some simulations of the CRPXY model we also use the parallel tempering method [70, 71]. It allows us to obtain results for small values of T , in particular below the Nishimori line $T = \sigma$. In the parallel-tempering simulations we consider N_T systems at the same value of σ and at N_T different inverse temperatures $\beta_{\min} \equiv \beta_1, \dots, \beta_{\max}$, where β_{\max} corresponds to the minimum value of the temperature we are interested in. The value β_{\min} is chosen so that thermalization at $\beta = \beta_{\min}$ is sufficiently fast, while the intermediate values β_i are chosen so that the acceptance probability of the temperature exchange is at least 5%. Moreover, we require that, for some i , $\beta_i = \sigma$. This allows us to collect data on the Nishimori line. The exact results valid on it allow us to check the correctness of the MC code and perform a (weak) test of thermalization. Thermalization is checked by verifying that the averages of the observables are independent of the number of MC steps for each disorder realization.

The overlap correlations and the corresponding χ_o and ξ_o are measured by performing two independent runs for each disorder sample. Finally, note that the determination of g_{22} defined in (14) requires the computation of the disorder average of products of thermal expectations. This should be done with care in order to avoid any bias due to the finite length of the run for each disorder realization. We use the essentially unbiased estimators discussed in [73, 72].

Appendix B. The KT RG equations

In this Appendix we consider the RG flow for the sine Gordon (SG) model, with the purpose of understanding its universal features. As a results we shall obtain the

critical behavior of the correlation length and of the magnetic susceptibility at the KT transition. This appendix generalizes the results presented in [74, 75, 76]. The SG model is parametrized by two couplings, α and δ —we use the notations of [74, 76]—whose β functions are

$$\beta_\alpha = 2\alpha\delta + \frac{5}{64}\alpha^3 + \dots, \quad (\text{B.1})$$

$$\beta_\delta = \frac{1}{32}\alpha^2 - \frac{1}{16}\alpha^2\delta + \dots, \quad (\text{B.2})$$

where the dots indicate higher-order terms. To all orders the β functions have the generic form

$$\beta_\alpha = 2\alpha\delta + \sum_{n+m>2} b_{\alpha,nm} \alpha^n \delta^m, \quad (\text{B.3})$$

$$\beta_\delta = \frac{1}{32}\alpha^2 + \sum_{n+m>2} b_{\delta,nm} \alpha^n \delta^m. \quad (\text{B.4})$$

In the SG model the sign of α is irrelevant, which implies the symmetry relations

$$\beta_\alpha(\alpha, \delta) = -\beta_\alpha(-\alpha, \delta), \quad \beta_\delta(\alpha, \delta) = \beta_\delta(-\alpha, \delta). \quad (\text{B.5})$$

As a consequence, $b_{\alpha,nm} = 0$ if n is even and $b_{\delta,nm} = 0$ if n is odd. Moreover, for $\alpha = 0$ the theory is free and δ does not flow. Hence

$$\beta_\delta(\alpha = 0, \delta) = 0, \quad (\text{B.6})$$

which implies $b_{\delta,nm} = 0$ if $n = 0$.

Let us now consider a general nonlinear analytic redefinition of the couplings

$$\alpha = a_{\alpha,10}u + \sum_{n+m\geq 2} a_{\alpha,nm} u^n v^m, \quad (\text{B.7})$$

$$\delta = a_{\delta,01}v + \sum_{n+m\geq 2} a_{\delta,nm} u^n v^m. \quad (\text{B.8})$$

We have verified up to the 7th order that with a proper choice of the coefficients $a_{\alpha,nm}$ and $a_{\delta,nm}$ one can rewrite the β functions in the form

$$\beta_u(u, v) = -uv, \quad (\text{B.9})$$

$$\beta_v(u, v) = -u^2(1 + b_1v + b_3v^3 + b_5v^5 + \dots). \quad (\text{B.10})$$

The couplings u and v are not uniquely defined and indeed there is a family of transformations that do not change the β functions (B.9) and (B.10). Extending the previous results to all orders, in the following we assume that we can choose u and v in such a way that $\beta_u(u, v)$ is given by (B.9) and $\beta_v(u, v)$ has the form

$$\beta_v(u, v) = -u^2[1 + vf(v^2)], \quad (\text{B.11})$$

where $f(v^2)$ is an analytic function in the region $v < v_0$, where v_0 is the starting point of the RG flow, and satisfies $1 + vf(v^2) > 0$ in this domain (if this were not true, we would have another nontrivial fixed point). This parametrization is unique (universal) in the sense that there is no analytic redefinition of the couplings which allows one to

write the β functions in the form (B.9), (B.11) with a different function $f(v^2)$, i.e. with different coefficients b_{2n+1} . The perturbative calculations of [74] allow us to determine b_1 :

$$b_1 = -\frac{3}{2}. \quad (\text{B.12})$$

The analysis of the flow in the general case is analogous to that presented in [74, 76]. First, we define the RG invariant function

$$\begin{aligned} Q(u, v) &= u^2 - F(v), \\ F(v) &= 2 \int_0^v \frac{w dw}{1 + w f(w^2)} = v^2 + v^3 + \frac{9}{8}v^4 + O(v^5), \end{aligned} \quad (\text{B.13})$$

which satisfies

$$\frac{dQ}{dl} = \frac{\partial Q}{\partial u} \beta_u(u, v) + \frac{\partial Q}{\partial v} \beta_v(u, v) = 0, \quad (\text{B.14})$$

where l is the flow parameter. The RG flow follows the lines $Q = \text{constant}$. It is thus natural to parametrize the RG flow in terms of Q and $v(l)$. Since

$$\frac{dv}{dl} = \beta_v(u, v) = -[Q + F(v)][1 + v f(v^2)], \quad (\text{B.15})$$

we obtain

$$l = - \int_{v_0}^v \frac{dw}{[Q + F(w)][1 + w f(w^2)]}, \quad (\text{B.16})$$

where $v(l=0) = v_0$.

Let us now apply these results to the XY model. Repeating the discussion of [77, 78] the XY model can be mapped onto a line in the (u, v) plane with $v > 0$. The KT transition is the intersection of this line with the line $Q = 0$ and the high-temperature phase corresponds to $Q > 0$. Thus, Q plays the role of thermal nonlinear scaling field, i.e.

$$Q = q_1 \tau + q_2 \tau^2 + \dots \quad (\text{B.17})$$

where $\tau = (T - T_{XY})/T_{XY}$.

To derive the expected critical behavior we consider the singular part of the free energy in a box of size L . It satisfies the scaling equation [79]

$$\mathcal{F}_{\text{sing}}(\tau, L) = e^{-2l} f(Q, v(l), e^{-l}L), \quad (\text{B.18})$$

where we have parametrized the flow in terms of Q and $v(l)$ and we have neglected all irrelevant operators. If $Q > 0$, as discussed in [74], $v(l)$ decreases continuously and $v(l) \rightarrow -\infty$ as $l \rightarrow \infty$. Since v_0 , the starting point of the flow, is positive, we can fix l by requiring

$$v(l) = -1, \quad (\text{B.19})$$

so that

$$l = \int_{-1}^{v_0} \frac{dw}{[Q + F(w)][1 + w f(w^2)]} = I(Q, v_0). \quad (\text{B.20})$$

It follows

$$\mathcal{F}_{\text{sing}}(\tau, L) = e^{-2I(Q, v_0)} f(Q, -1, e^{-I(Q, v_0)} L), \quad (\text{B.21})$$

which gives the scaling behavior of the free energy (using $Q \sim \tau$). In the scaling limit the finite-size dependence can be parametrized in terms of ξ/L , where ξ is the correlation length. This allows us to identify

$$\xi(\tau) = \xi_0 e^{I(Q, v_0)}, \quad (\text{B.22})$$

where ξ_0 is a constant. The behavior of $\xi(\tau)$ for $\tau \rightarrow 0$ is obtained by expanding $I(Q, v_0)$ for $Q \rightarrow 0$. The generic behavior is

$$I(Q, v_0) = \frac{1}{\sqrt{Q}} \sum_n I_n Q^n + \sum_n I_{\text{an},n}(v_0) Q^n. \quad (\text{B.23})$$

The nonanalytic terms in the expansion depend only of the coefficients b_{2n+1} which appear in (B.10). The first two coefficients are

$$\begin{aligned} I_0 &= \pi, \\ I_1 &= \frac{\pi b_1}{4} = \frac{9\pi}{16}. \end{aligned} \quad (\text{B.24})$$

Correspondingly, we obtain

$$\xi(\tau) = X \exp(\pi/\sqrt{Q}) [1 + I_1 \sqrt{Q} + O(Q)]. \quad (\text{B.25})$$

Expanding Q in powers of τ we obtain the celebrated KT expression for the correlation length.

Let us now consider the behavior of the susceptibility. Perturbation theory gives for the scaling dimension of the spin correlation function [74]

$$\gamma = -\frac{1}{4} + \frac{1}{4}\delta - \frac{1}{4}\delta^2 + h_1 \alpha^2 + \dots, \quad (\text{B.26})$$

where h_1 is an unknown coefficient. If we perform the redefinitions $(\alpha, \delta) \rightarrow (u, v)$ considered before, we can rewrite γ as[¶]

$$\gamma = -\frac{1}{4} - \frac{1}{8}v - \frac{1}{16}v^2 + \dots \quad (\text{B.27})$$

without the α^2 term. In the infinite-volume limit the susceptibility satisfies the scaling law

$$\chi \xi^{-7/4} = A \exp \left[\int_{v_0}^{v(l)} \frac{\gamma(w) + 1/4}{\beta_v} dw \right] G_\chi[Q, v(l)], \quad (\text{B.28})$$

the integral is computed at fixed Q with β_v given by (B.15), and G_χ is an analytical function. Setting $v(l) = -1$ and expanding the integral in powers of Q , we obtain an expansion of the form

$$\chi \xi^{-7/4} = A(1 + c_1 \sqrt{Q} + c_2 Q + \dots). \quad (\text{B.29})$$

[¶] The possibility of cancelling the term of order α^2 is related to the existence of a family of transformations, given at second order by $u' = u + Au v$, $v' = v + Au^2$ with arbitrary A , which leave invariant the β -functions (B.9) and (B.10). By properly choosing A one can eliminate the α^2 term in $\gamma(u', v')$.

The coefficient c_1 can be computed exactly using the perturbative results (B.10), (B.12), and (B.27), obtaining

$$c_1 = \frac{\pi}{16}. \quad (\text{B.30})$$

Using (B.25) we can write

$$\sqrt{Q} = \frac{\pi}{\ln \xi/X} + O(\ln^{-3} \xi) \quad (\text{B.31})$$

and obtain

$$\chi \xi^{-7/4} = A_\chi \left[1 + \frac{\pi^2}{16 \ln(\xi/X)} + O(1/\ln^2 \xi) \right]. \quad (\text{B.32})$$

Note that the leading logarithmic scaling correction has a universal coefficient. We should note that in [76] it was incorrectly claimed that $c_1 = 0$ and, as a consequence, that the leading scaling corrections in (B.32) are proportional to $1/(\ln \xi)^2$. We numerically checked (B.32) by fitting the infinite-volume numerical data of [67] (more precisely their data for $\beta \geq 0.92$, corresponding to $10 \lesssim \xi \lesssim 420$) to

$$\ln(\chi \xi^{-7/4}) = a + \frac{b}{\ln(\xi/X)}, \quad (\text{B.33})$$

obtaining $a = 0.804(2)$ and $b = 0.627(9)$ (with $\chi^2/\text{DOF} \approx 0.7$), which is perfectly consistent with the value of b obtained in perturbation theory, i.e. $b = \pi^2/16 \approx 0.617$ (fixing $b = \pi^2/16$, we obtain $a = 0.8058(1)$ with $\chi^2/\text{DOF} \approx 0.7$, while a fit to $a + b/\ln(\xi/X) + c/\ln^2(\xi/X)$ gives $a = 0.8046(9)$, $c = 0.029(22)$ with $\chi^2/\text{DOF} \approx 0.6$, which confirms that the next-to-leading correction is very small in (B.33)).

The result (B.32) is general. If \mathcal{O} is a generic long-distance quantity which behaves as ξ_o^x in the critical limit, we expect \mathcal{O}/ξ_o^x to behave as $\chi/\xi^{7/4}$, i.e. to satisfy a relation analogous to (B.28). It is only needed to replace $\gamma(u, v) + 1/4$ with the appropriate subtracted scaling dimension. Thus, \mathcal{O}/ξ_o^x also has an expansion of the form (B.32), i.e.

$$\mathcal{O} = \xi_o^x \left[1 + \frac{c_{\mathcal{O}}}{\ln \xi/X} + O(\ln^{-2} \xi) \right], \quad (\text{B.34})$$

where $c_{\mathcal{O}}$ is universal and can be computed by using the perturbative expression of the scaling dimension of \mathcal{O} . More precisely, if the scaling dimension $\gamma_{\mathcal{O}}(u, v)$ has the perturbative expansion

$$\gamma_{\mathcal{O}}(u, v) = g_{00} + g_{01}v + g_{02}v^2 + g_{20}u^2 + \dots \quad (\text{B.35})$$

we obtain

$$c_{\mathcal{O}} = -\pi g_{02}. \quad (\text{B.36})$$

Corrections proportional to $1/\ln \xi/X$ should instead be absent in RG invariant quantities. Indeed, if R is such a quantity, if we neglect the scaling corrections, R satisfies the scaling relation

$$R(\tau) = G_R[Q, v(l)], \quad (\text{B.37})$$

for any l . This implies that $R(\tau)$ is independent of $v(l)$, hence an analytic function of Q and therefore of τ . It follows

$$R(\tau) = R^* + \frac{c_R}{\ln^2 \xi / X} + O(\ln^{-4} \xi), \quad (\text{B.38})$$

where the constant c_R is expected to be universal.

Appendix C. General behavior close to a critical point

Let us consider a multicritical point in a two-parameter space labelled by T and σ and let us assume that the correlation length behaves as

$$\xi(T, \sigma) \sim [T - T_c(0)]^{-\nu_1} \quad \sigma = 0, \quad (\text{C.1})$$

$$\xi(T, \sigma) \sim [T - T_c(\sigma)]^{-\nu_2} \quad \sigma > 0, \quad (\text{C.2})$$

where $T_c(\sigma)$ is the σ -dependent critical point and $\nu_1 \neq \nu_2$. According to the RG, close to the multicritical point $\xi(T, \sigma)$ behaves as

$$\xi(T, \sigma) = u_t(T, \sigma)^{-\nu_m} F[u_\sigma(T, \sigma) u_t(T, \sigma)^{-\phi}], \quad (\text{C.3})$$

where $u_\sigma(T, \sigma)$ and $u_t(T, \sigma)$ are the scaling fields and ϕ and ν_m two critical exponents. Since one of the two scaling fields must vanish along the transition line, we define $u_t(T, \sigma)$ as the scaling field which has this property. Therefore, we define

$$u_t(T, \sigma) = \frac{T - T_c(\sigma)}{T_c(0)}. \quad (\text{C.4})$$

For $\sigma \rightarrow 0$ and $T \rightarrow T_c(0)$, it behaves as

$$u_t(T, \sigma) = \tau + c_\sigma \sigma + \dots \quad \tau \equiv \frac{T - T_c(0)}{T_c(0)}. \quad (\text{C.5})$$

We assume that $c_\sigma \neq 0$, i.e. that the transition line is not perpendicular to the line $\sigma = 0$, as it occurs in the RPXY model. Finally, we note that $u_\sigma(T, \sigma)$ does not vanish on the transition line, unless $\sigma = 0$.

Now consider $T \rightarrow T_c(\sigma)$ at fixed nonvanishing σ . Since $u_\sigma(T, \sigma) \neq 0$ we obtain (C.2) only if

$$F(x) \sim x^\lambda \quad \lambda = \frac{\nu_2 - \nu_m}{\phi} \quad (\text{C.6})$$

for $x \rightarrow \infty$. To go further let us distinguish two cases: (i) $u_\sigma(T, \sigma)$ vanishes identically for $\sigma = 0$, i.e. $u_\sigma(T, 0) = 0$ for any T ; (ii) $u_\sigma(T, 0)$ is different from zero unless $T = T_c(\sigma = 0)$.

In case (i) (C.1) requires

$$F(0) \neq 0, \quad \nu_m = \nu_1. \quad (\text{C.7})$$

Assuming $u_\sigma(T = T_c(0), \sigma) = d_\sigma \sigma$ for $\sigma \rightarrow 0$ we obtain

$$\xi(T = T_c(0), \sigma) = (c_\sigma \sigma)^{-\nu_1} F(d_\sigma c_\sigma^{-\phi} \sigma^{1-\phi}). \quad (\text{C.8})$$

The observed behavior depends on the value of ϕ . For $\phi < 1$, since $F(0) \neq 0$ we obtain

$$\xi(T = T_c(0), \sigma) = (c_\sigma \sigma)^{-\nu_1} (a + b\sigma^{1-\phi} + \dots) \quad (\text{C.9})$$

The corrections are correct provided that $F(x)$ is analytic for $x = 0$. If $\phi > 1$, using (C.6) we obtain the behavior

$$\xi(T = T_c(0), \sigma) \sim \sigma^{-\bar{\nu}} \quad \bar{\nu} = \nu_1 - (1 - \phi)\lambda = \frac{\nu_2(\phi - 1) + \nu_1}{\phi}. \quad (\text{C.10})$$

In case (ii), if $u_\sigma(T, \sigma = 0) = d_T \tau + O(\tau^2)$ we obtain for $\sigma = 0$

$$\xi(T, 0) = \tau^{-\nu_m} F(d_T \tau^{1-\phi}), \quad (\text{C.11})$$

which shows that

$$F(d_T \tau^{1-\phi}) \sim \tau^{\nu_m - \nu_1} \quad (\text{C.12})$$

in the limit $\tau \rightarrow 0$. Let us now consider the behavior for $T = T_c(0)$ as a function of σ . For $\sigma \rightarrow 0$ we have

$$\xi(T = T_c(0), \sigma) = c_\sigma^{-\nu_m} \sigma^{-\nu_m} F(d_\sigma c_\sigma^{-\phi} \sigma^{1-\phi}) \sim \sigma^{-\nu_1}, \quad (\text{C.13})$$

where we have used relation (C.12). Thus, in case (ii) we have $\xi(T = T_c(0), \sigma) \sim \sigma^{-\nu_1}$ for any value of ϕ .

Let us now show that the case relevant for the RPXY model is case (i). Indeed, case (ii) can only occur if the two relevant operators which occur at the multicritical point are both present in the model at $\sigma = 0$. This does certainly not occur in our case in which σ is associated with randomness. Therefore, our result that in the RPXY model $\xi(T = T_c(0), \sigma)$ behaves as $\sigma^{-\nu_1}$ implies that $\phi < 1$, i.e. that the RG dimension of the new operator that arises in the theory with $\sigma \neq 0$ is less relevant than the thermal operator present at $\sigma = 0$. This is also the case of three-dimensional randomly dilute Ising systems or $\pm J$ Ising models at their ferromagnetic transitions at small disorder. Indeed, the crossover from the pure critical behavior to that of the randomly-dilute Ising universality class is described by the crossover exponent $\phi = \alpha_{\text{Is}} = 0.1096(5)$ [69, 80], see also the discussion reported in [81].

Similar considerations apply to other quantities. For instance, consider a RG invariant quantity R . It behaves as

$$R(T, \sigma) = r[u_\sigma(T, \sigma)u_t(T, \sigma)^{-\phi}]. \quad (\text{C.14})$$

If $\phi < 1$, $R(T, \sigma)$ approaches the same value R^* along the lines $\sigma = 0$ and $T = T_c(0)$. Moreover, in the second case we expect corrections of the form

$$R(T_c(0), \sigma) = R^* + a\sigma^{1-\phi} + \dots = R^* + a'\xi^{(\phi-1)/\nu_1} + \dots \quad (\text{C.15})$$

Appendix D. RG equations in the presence of randomness

The RG equations in the small disorder regime and close to the paramagnetic-QLRO transition line have been derived in [3, 23, 28, 31, 35]:

$$\begin{aligned}\frac{dT}{dl} &= -4\pi^3 Y^2, \\ \frac{d\sigma}{dl} &= 0, \\ \frac{dY}{dl} &= (2 - \pi\beta + \pi\sigma\beta^2)Y,\end{aligned}$$

where Y is the vorticity and only terms up to $O(Y^2)$ are kept. Let us now redefine the couplings as follows:

$$\begin{aligned}T^{-1} &= \frac{1}{\pi}(2 + v + \sigma), \\ Y &= \frac{u}{4\pi}.\end{aligned}\tag{D.1}$$

For $u, v \rightarrow 0$ the RG equations become

$$\begin{aligned}\frac{du}{dl} &= -uv, \\ \frac{dv}{dl} &= -u^2, \\ \frac{d\sigma}{dl} &= 0.\end{aligned}\tag{D.2}$$

We have thus reobtained the RG equations for the XY model. This implies that, in the region of couplings in which (D.2) hold, the RG behavior is analogous to that close to the KT fixed point, apart from an analytic redefinition of the scaling fields.

Appendix E. Magnetic correlations in the gauge-glass model

For the gauge-glass model ($\sigma = \infty$) we can derive some identities which relate magnetic and overlap quantities. The basic observation is that for $\sigma = +\infty$ the distribution function of the A_{xy} variables is gauge-invariant. Hence we have

$$[\langle \psi_{x_1}^* \dots \psi_{x_n}^* \psi_{y_1} \dots \psi_{y_n} \rangle] = V_{x_1}^* \dots V_{x_n}^* V_{y_1} \dots V_{y_n} [\langle \psi_{x_1}^* \dots \psi_{x_n}^* \psi_{y_1} \dots \psi_{y_n} \rangle] \tag{E.1}$$

for any set of phases V_x . It implies that magnetic correlations vanish unless each x_i is equal to some y_j . Analogously we have

$$\begin{aligned}[\langle \psi_{x_1}^* \dots \psi_{x_n}^* \psi_{y_1} \dots \psi_{y_n} \rangle \langle \psi_{z_1}^* \dots \psi_{z_n}^* \psi_{t_1} \dots \psi_{t_n} \rangle] &= \\ &= V_{x_1}^* \dots V_{x_n}^* V_{y_1} \dots V_{y_n} V_{z_1}^* \dots V_{z_n}^* V_{t_1} \dots V_{t_n} [\langle \psi_{x_1}^* \dots \psi_{x_n}^* \psi_{y_1} \dots \psi_{y_n} \rangle \langle \psi_{z_1}^* \dots \psi_{z_n}^* \psi_{t_1} \dots \psi_{t_n} \rangle].\end{aligned}\tag{E.2}$$

These relations allow us to write

$$[\langle \psi_x^* \psi_y \rangle] = \delta_{xy}, \tag{E.3}$$

$$[\langle \psi_{x_1}^* \psi_{x_2}^* \psi_{y_1} \psi_{y_2} \rangle] = \delta_{x_1 y_1} \delta_{x_2 y_2} + \delta_{x_1 y_2} \delta_{x_2 y_1} - \delta_{x_1 y_1} \delta_{x_1 x_2} \delta_{x_1 y_2}, \tag{E.4}$$

$$[\langle \psi_{x_1}^* \psi_{y_1} \rangle \langle \psi_{x_2}^* \psi_{y_2} \rangle] = \delta_{x_1 y_1} \delta_{x_2 y_2} + \delta_{x_1 y_2} \delta_{x_2 y_1} [|\langle \psi_{x_1}^* \psi_{y_1} \rangle|^2] - \delta_{x_1 y_1} \delta_{x_1 x_2} \delta_{x_1 y_2} \tag{E.5}$$

It follows

$$\begin{aligned} [\langle |\mu|^2 \rangle] &= V, \\ [\langle |\mu|^4 \rangle] &= 2V^2 - V, \\ [\langle |\mu|^2 \rangle^2] &= V^2 + V^2 \chi_o - V, \end{aligned} \tag{E.6}$$

which imply

$$\begin{aligned} \chi &= 1, \\ \chi_4 &= 1 - 2\chi_o, \\ \chi_{22} &= \chi_o - 1. \end{aligned} \tag{E.7}$$

Moreover, it is easy to show that $\xi = 0$. Relations (E.7) show that χ_4 and χ_{22} both diverge as χ_o . In the critical limit we have $\chi_o \sim \xi_o^2$ because $\eta_o = 0$. Therefore we can write

$$\chi_4 \approx -2a\xi_o^2, \quad \chi_{22} \approx a\xi_o^2, \tag{E.8}$$

for $\xi_o \rightarrow \infty$, where a is constant.

We shall now assume that these results are valid for the whole universality class: for any $\sigma > \sigma_D$, relations (E.8) always hold with a constant a which in general depends on σ . We can reexpress these results in terms of the quartic couplings. If we use (E.8) we have

$$g_4 = \frac{3a\xi_o^2}{\chi^2\xi^2}, \tag{E.9}$$

$$g_{22} = -\frac{a\xi_o^2}{\chi^2\xi^2}, \tag{E.10}$$

Since the magnetic susceptibility χ and correlation length ξ are finite and nonzero (except for $\sigma = \infty$, where anyhow the quartic couplings are not well-defined since $\xi = 0$ for any L), we expect that g_4 and g_{22} diverge as ξ_o^2 in the critical limit. As for $g_c = g_4 + 3g_{22}$, (E.10) shows that the leading ξ_o^2 term cancels. Since in the calculation we have neglected the scaling corrections to (E.8), this does not necessarily imply that g_c remains finite in the critical limit, but only that $g_c \xi_o^{-2} \rightarrow 0$ as $\xi_o \rightarrow \infty$. The exact behavior depends on the neglected scaling corrections. These predictions are confirmed by our numerical results, see Sec. 6.7. It is worth mentioning that this behavior is analogous to that observed in the 2D Ising spin glass model, where χ_4 behaves as χ_o and thus diverges approaching the glassy transition; see, e.g., [82] and references therein.

References

- [1] Granato E and Kosterlitz J M 1986 Quenched disorder in Josephson-junction arrays in a transverse magnetic field *Phys. Rev. B* **33** 6533
- [2] Granato E and Kosterlitz J M 1989 Disorder in Josephson-junction arrays in a magnetic field *Phys. Rev. Lett.* **62** 823
- [3] Rubinstein M, Shrainam B and Nelson D R 1983 Two-dimensional XY magnets with random Dzyaloshinskii-Moriya interactions *Phys. Rev. B* **27** 1800

- [4] Cha M-C and Fertig H A 1994 Orientational order and depinning of the disordered electron solid *Phys. Rev. Lett.* **73** 870 [arXiv:cond-mat/9402021]
Cha M-C and Fertig H A 1994 Topological defects, orientational order, and depinning of the electron solid in a random potential *Phys. Rev. B* **50** 14368 [arXiv:cond-mat/9409001]
- [5] Fisher M P A, Tokuyasu T A and Young A P 1991 Vortex variable-range-hopping resistivity in superconducting films *Phys. Rev. Lett.* **66** 2931
- [6] Korshunov S E 2006 Phase transitions in two-dimensional systems with continuous degeneracy *Usp. Fiz. Nauk* **176** 233, *Physics Uspekhi* **49** 225 (English translation)
- [7] Kawashima N and Rieger H 2004 Recent Progress in Spin Glasses in *Frustrated Spin Systems* ed H T Diep (World Scientific: Singapore) [arXiv:cond-mat/0312432]
- [8] Ozeki Y and Nishimori H 1993 Phase diagram of gauge glasses *J. Phys. A: Math. Gen.* **26** 3399
- [9] Nishimori H 2002 Exact results on spin glass models *Physica A* **306** 68 [arXiv:cond-mat/0201056]
- [10] Ebner C and Stroud D 1985 Diamagnetic susceptibility of superconducting clusters: Spin-glass behavior *Phys. Rev. B* **31** 165
- [11] Forrester M G, Lee Hu Jong, Tinkhams M and Lobb C J 1988 Positional disorder in Josephson-junction arrays: Experiments and simulations *Phys. Rev. B* **37** 5966
- [12] Chakrabarti A and Dasgupta C 1988 Phase transition in positionally disordered Josephson-junction arrays in a transverse magnetic field *Phys. Rev. B* **37** 7557
- [13] Forrester M G, Benz S P and Lobb C J 1990 Monte Carlo simulations of Josephson-junction arrays with positional disorder *Phys. Rev. B* **41** 8749
- [14] Huse D A and Seung H S 1990 Possible vortex-glass transition in a model random superconductor *Phys. Rev. B* **42** 1059
- [15] Reger J D, Tokuyasu T A, Young A P and Fisher M P A 1991 Vortex-glass transition in three dimensions *Phys. Rev. B* **44** 7147
- [16] Li Y-H 1992 Voltage-current characteristics of the two-dimensional gauge glass model *Phys. Rev. Lett.* **69** 1819
- [17] Gingras M J P 1992 Numerical study of vortex-glass order in random-superconductor and related spin-glass models *Phys. Rev. B* **45** 7547
- [18] Dekker C, Wöltgens P J M, Koch R H, Hussey B W and Gupta A 1992 Absence of a finite-temperature vortex-glass phase transition in two-dimensional $\text{YBa}_2\text{Cu}_3\text{O}_{7-\delta}$ films *Phys. Rev. Lett.* **69** 2717
- [19] Reger J D and Young A P 1993 Monte Carlo study of a vortex glass model *J. Phys. A: Math. Gen.* **26** L1067 [arXiv:cond-mat/9311036]
- [20] Korshunov S E 1993 Possible destruction of the ordered phase in Josephson-junction arrays with positional disorder *Phys. Rev. B* **48** 1124
- [21] Nishimori H and Kawamura H 1993 Gauge glass ordering in two dimensions *J. Phys. Soc. Jpn.* **62** 3266
- [22] Nishimori H 1994 Gauge glass, spin glass and coding theory: Exact results *Physica A* **205** 1
- [23] Nattermann T, Scheidl S, Korshunov S E and Li M S 1995 Absence of reentrance in the two-dimensional XY model with random phase shifts *J. Physique I (France)* **5** 565 [arXiv:cond-mat/9501120]
- [24] Cha M-C and Fertig H A 1995 Disorder-induced phase transitions in two-dimensional crystals *Phys. Rev. Lett.* **74** 4867
- [25] Jeon G S, Kim S and Choi M Y 1995 Phase transition in the XY gauge glass *Phys. Rev. B* **51** 16211
- [26] Hyman R A, Wallin M, Fisher M P A, Girvin S M and Young A P 1995 Current-voltage characteristics of two-dimensional vortex-glass models *Phys. Rev. B* **51** 15304 [arXiv:cond-mat/9409117]
- [27] Korshunov S E and Nattermann T 1996 Absence of reentrance in superconducting arrays with positional disorder *Phys. Rev. B* **53** 2746
- [28] Tang L-H 1996 Vortex statistics in a disordered two-dimensional XY model *Phys. Rev. B* **54** 3350

- [arXiv:cond-mat/9602162]
- [29] Bokil H S and Young A P 1996 Study of chirality in the two-dimensional XY spin glass *J. Phys. A: Math. Gen.* **29** L89 [arXiv:cond-mat/9512042]
- [30] Maucourt J and Gempel D R 1997 Phase transitions in the two-dimensional XY model with random phases: A Monte Carlo study. *Phys. Rev. B* **56** 2572 [arXiv:cond-mat/9703109]
- [31] Scheidl S 1997 Glassy vortex state in a two-dimensional disordered XY model *Phys. Rev. B* **55** 457 [arXiv:cond-mat/9601131]
- [32] Kosterlitz J M and Simkin M V 1997 Numerical study of a superconducting glass model *Phys. Rev. Lett.* **79** 1098 [arXiv:cond-mat/9702166]
- [33] Kim B J, Choi M Y, Ryu S and Stroud D 1997 Anomalous relaxation in the XY gauge glass *Phys. Rev. B* **56** 6007 [arXiv:cond-mat/9707140]
- [34] Maucourt J and Gempel D R 1998 Scaling of domain-wall energies in the three-dimensional gauge glass model *Phys. Rev. B* **58** 2654
- [35] Carpentier D and Le Doussal P 1998 Disordered XY models and Coulomb gases: Renormalization via traveling waves *Phys. Rev. Lett.* **81** 2558 [arXiv:cond-mat/9802083]
- [36] Granato E 1998 Current-voltage scaling of chiral and gauge-glass models of two-dimensional superconductors *Phys. Rev. B* **58** 11161 [arXiv:cond-mat/9808331]
- [37] Sawa A, Yamasaki H, Mawatari Y, Obara H, Umeda M and Kosaka S 1998 Thickness dependence of the vortex-glass transition and critical scaling of current-voltage characteristics in $\text{YBa}_2\text{Cu}_3\text{O}_{7-\delta}$ thin films *Phys. Rev. B* **58** 2868
- [38] Kosterlitz J M and Akino N 1999 Numerical study of spin and chiral order in a two-dimensional XY spin glass *Phys. Rev. Lett.* **82** 4094 [arXiv:cond-mat/9806339]
- [39] Mudry C and Wen X-G 1999 Does quasi-long-range order in the two-dimensional XY model really survive weak random phase fluctuations? *Nucl. Phys. B* **549** 613 [arXiv:cond-mat/9712146]
- [40] Choi M Y and Park S Y 1999 Phase transition in the two-dimensional gauge glass *Phys. Rev. B* **60** 4070 [arXiv:cond-mat/9906326]
- [41] Kim B J 2000 Finite-temperature resistive transition in the two-dimensional XY gauge glass model *Phys. Rev. B* **62** 644 [arXiv:cond-mat/0004069]
- [42] Carpentier D and Le Doussal P 2000 Topological transitions and freezing in XY models and Coulomb gases with quenched disorder: renormalization via traveling waves *Nucl. Phys. B* **588** 565 [arXiv:cond-mat/9908335]
- [43] Akino N and Kosterlitz J M 2002 Domain wall renormalization group study of the XY model with quenched random phase shifts *Phys. Rev. B* **66** 054536 [arXiv:cond-mat/0203299]
- [44] Holme P and Olsson P 2002 A zero-temperature study of vortex mobility in two-dimensional vortex glass models *Europhys. Lett.* **60** 439 [arXiv:cond-mat/0111555]
- [45] Katzgraber H G and Young A P 2002 Numerical studies of the two- and three-dimensional gauge glass at low temperature *Phys. Rev. B* **66** 224507 [arXiv:cond-mat/0205206]
- [46] Katzgraber H G 2003 On the existence of a finite-temperature transition in the two-dimensional gauge glass *Phys. Rev. B* **67** 180402(R) [arXiv:cond-mat/0305393]
Katzgraber H G 2003 Numerical studies of the two- and three-dimensional gauge glass at low temperature *J. Applied Phys.* **93** 7661 [arXiv:cond-mat/0304540]
- [47] Holme P, Kim B J and Minnhagen P 2003 Phase transitions in the two-dimensional random gauge XY model *Phys. Rev. B* **67** 104510 [arXiv:cond-mat/0301279]
- [48] Chen Q-H, Tanaka A and Hu X 2003 Evidence for finite-temperature glass transition in two dimensions *Physica B* **329** 1413
- [49] Nikolaou M and Wallin M 2004 Zero-temperature glass transition in the two-dimensional gauge glass model *Phys. Rev. B* **69** 184512 [arXiv:cond-mat/0312066]
- [50] Katzgraber H G and Campbell I A 2005 Dynamical scaling in Ising and vector spin glasses *Phys. Rev. B* **72** 014462 [arXiv:cond-mat/0504082]
- [51] Tang L-H and Tong P 2005 Zero-temperature criticality in the two-dimensional gauge glass model *Phys. Rev. Lett.* **94** 207204 [arXiv:cond-mat/0412415]

- [52] Um J, Kim B J, Minnaghen P, Choi M Y and Lee S-I 2006 Dynamic critical behaviors in two-dimensional Josephson junction arrays with positional disorder *Phys. Rev. B* **74** 094516 [arXiv:cond-mat/0608390]
- [53] Yun Y J, Baek I C and Choi M Y 2006 Experimental study of positionally disordered Josephson junction arrays *Europhys. Lett.* **76** 271 [arXiv:cond-mat/0509151]
- [54] Chen Q-H, Lv J-P and Liu H 2008 Dynamics of glass phases in the two-dimensional gauge glass model *Phys. Rev. B* **78** 054519 [arXiv:0812.2822]
- [55] Alba V, Pelissetto A and Vicari E 2009 Quasi-long-range order in the 2D XY model with random phase shifts *J. Phys.: Math. Gen. A* **42** 295001 [arXiv:0901.4682]
- [56] Kosterlitz J M and Thouless D J 1973 Ordering, metastability and phase transitions in two-dimensional systems *J. Phys. C: Solid State* **6** 1181
- [57] Hasenbusch M and Pinn K 1997 Computing the roughening transition of Ising and solid-on-solid models by BCSOS model matching *J. Phys. A: Math. Gen.* **30** 63 [arXiv:cond-mat/9605019]
Hasenbusch M, Marcu M and Pinn K 1994 High-precision renormalization-group study of the roughening transition *Physica A* **208** 124 [arXiv:hep-lat/9404016]
- [58] Nishimori H 1981 Internal energy, specific heat and correlation function of the bond-random Ising model *Prog. Theor. Phys.* **66** 1169
- [59] Hasenbusch M, Parisen Toldin F, Pelissetto A and Vicari E 2008 Multicritical Nishimori point in the phase diagram of the $\pm J$ Ising model on a square lattice *Phys. Rev. E* **77** 051115 [arXiv:0803.0444]
- [60] Picco M, Honecker A and Pujol P 2006 Strong disorder fixed points in the two-dimensional random-bond Ising model *J. Stat. Mech.: Theory Exp.* P09006 [arXiv:cond-mat/0606312]
- [61] Hasenbusch M, Parisen Toldin F, Pelissetto A and Vicari E 2008 Universal dependence on disorder of two-dimensional randomly diluted and random-bond $\pm J$ Ising models *Phys. Rev. E* **78** 011110 [arXiv:0804.2788]
- [62] Parisen Toldin F, Pelissetto A and Vicari E 2009 Strong-Disorder Paramagnetic-Ferromagnetic Fixed Point in the Square-Lattice $\pm J$ Ising Model *J. Stat. Phys.* **135** 1039 [arXiv:0811.2101]
- [63] Parisen Toldin F, Pelissetto A and Vicari E 2010 in preparation.
- [64] Amoruso C and Hartmann A K 2004 Domain-wall energies and magnetization of the two-dimensional random-bond Ising model *Phys. Rev. B* **70** 134425 [arXiv:cond-mat/0401464]
- [65] Wang C, Harrington J and Preskill J 2003 Confinement-Higgs transition in a disordered gauge theory and the accuracy threshold for quantum memory *Ann. Phys. (NY)* **303** 31 [arXiv:quant-ph/0207088]
- [66] Campostrini M, Pelissetto A, Rossi P and Vicari E 1996 Strong-coupling analysis of two-dimensional $O(N)$ models with $N \leq 2$ on square, triangular, and honeycomb lattices *Phys. Rev. B* **54** 7301 [arXiv:hep-lat/9603002]
- [67] Balog J, Niedermaier M, Niedermayer F, Patrascioiu A, Seiler E and Weisz P 2001 Does the XY model have an integrable continuum limit? *Nucl. Phys. B* **618** 315 [arXiv:hep-lat/0106015]
- [68] Pelissetto A and Vicari E 2000 The effective potential of N-vector models: a field-theoretic study to $O(\epsilon^3)$ *Nucl. Phys. B* **575** 579 [arXiv:cond-mat/9911452]
Pelissetto A and Vicari E 1998 Four-point renormalized coupling constant and Callan-Symanzik β -function in $O(N)$ models *Nucl. Phys. B* **519** 123 [arXiv:cond-mat/9711078]
- [69] Pelissetto A and Vicari E 2002 Critical phenomena and renormalization-group theory *Phys. Rep.* **368** 549 [arXiv:cond-mat/0012164]
- [70] Geyer C J 1991 Markov chain Monte Carlo maximum likelihood in *Computer Science and Statistics: Proc. of the 23rd Symposium on the Interface*, ed E M Keramidas, p 156 (Interface Foundation: Fairfax Station, VA, USA)
Hukushima K and Nemoto K 1996 Exchange Monte Carlo method and application to spin glass simulations *J. Phys. Soc. Jpn.* **65** 1604
- [71] Earl D J and Deem M W 2005 Parallel tempering: Theory, applications, and new perspectives *Phys. Chem. Chem. Phys.* **7** 3910 [arXiv:physics/0508111]

- [72] Hasenbusch M, Pelissetto A and Vicari E 2008 Critical behavior of three-dimensional Ising spin glass models *Phys. Rev. B* **78** 214205 [arXiv:0809.3329]
Hasenbusch M, Pelissetto A and Vicari E 2008 The critical behavior of 3D Ising spin glass models: Universality and scaling corrections *J. Stat. Mech.: Theory Expt.* L02001 [arXiv:0710.1980]
- [73] Hasenbusch M, Parisen Toldin F, Pelissetto A and Vicari E 2007 The universality class of 3D site-diluted and bond-diluted Ising systems *J. Stat. Mech.: Theory Exp.* P02016 [arXiv:cond-mat/0611707]
- [74] Amit D J, Goldschmidt Y Y and Grinstein G 1980 Renormalisation group analysis of the phase transition in the 2D Coulomb gas, Sine-Gordon theory and XY-model *J. Phys.: Math. Gen. A* **13** 585
- [75] Balog J and Hegedüs A 2000 Two-loop beta-functions of the sine-Gordon model *J. Phys.: Math. Gen. A* **33** 6543 [arXiv:hep-th/0003258]
- [76] Balog J 2001 Kosterlitz-Thouless theory and lattice artifacts *J. Phys.: Math. Gen. A* **34** 5237 [arXiv:hep-lat/0011078]
- [77] Kosterlitz J M 1974 The critical properties of the two-dimensional xy model *J. Phys. C: Solid State Phys.* **7** 1046
- [78] José J V, Kadanoff L P, Kirkpatrick S and Nelson D R 1978 Renormalization, vortices, and symmetry-breaking perturbations in the two-dimensional planar model *Phys. Rev. B* **16** 1217
- [79] Wegner F J 1976 The Critical State, General Aspects in Phase Transitions and Critical Phenomena, Vol 6, ed C Domb and M Green, p 7 (Academic: New York)
- [80] Campostrini M, Pelissetto A, Rossi P and Vicari E 2002 25th-order high-temperature expansion results for three-dimensional Ising-like systems on the simple-cubic lattice *Phys. Rev. E* **65** 066127 [arXiv:cond-mat/0201180]
- [81] Hasenbusch M, Parisen Toldin F, Pelissetto A and Vicari E 2007 Magnetic-glassy multicritical behavior of the three-dimensional $\pm J$ Ising model *Phys. Rev. B* **76** 184202 [arXiv:0707.2866]
- [82] Binder K and Young A P 1986 Spin glasses: Experimental facts, theoretical concepts, and open questions *Rev. Mod. Phys.* **58** 801